ChemPubSoc Europe

DOI: 10.1002/cmdc.201300288

Synthesis, G-Quadruplex Stabilisation, Docking Studies, and Effect on Cancer Cells of Indolo[3,2-*b*]quinolines with One, Two, or Three Basic Side Chains

João Lavrado,[a] Pedro M. Borralho,[b, c] Stephan A. Ohnmacht,[d] Rui E. Castro,[b, c] Cecília M. P. Rodrigues,[b, c] Rui Moreira,[a] Daniel J. V. A. dos Santos,[a, e] Stephen Neidle,[d] and Alexandra Paulo*[a]

G-quadruplex (G4) DNA structures in telomeres and oncogenic promoter regions are potential targets for cancer therapy, and G4 ligands have been shown to modulate telomerase activity and oncogene transcription. Herein we report the synthesis and G4 thermal stabilisation effects, determined by FRET melting assays, of 20 indolo[3,2-*b*]quinolines mono-, di-, and trisubstituted with basic side chains. Molecular modelling studies were also performed in an attempt to rationalise the ligands' binding poses with G4. Overall, the results suggest that ligand binding and G4 DNA thermal stabilisation increase with an N5-methyl or a 7-carboxylate group and propylamine side chains, whereas selectivity between G4 and duplex DNA appears to be modulated by the number and relative position of basic side chains. From all the indoloquinoline derivatives studied, the novel trisubstituted compounds **3d** and **4d**, bearing a 7-(aminoalkyl)carboxylate side chain, stand out as the most promising compounds; they show high G4 thermal stabilisation (ΔT_m values between 17 and 8 °C) with an inter-G4 ΔT_m trend of *Hsp90A* > *KRas21R* ≈ F21T > *c-Kit2*, 10-fold selectivity for G4 over duplex DNA, and 100-fold selectivity for the HCT116 cancer cell line (IC_{50} and IC_{90}: < 10 μM) over primary rat hepatocytes. Compounds **3d** and **4d** also decreased protein expression levels of Hsp90 and KRas in HCT116 cancer cells.

Introduction

Nucleic acid sequences containing repetitive guanine (G)-rich tracts can form G-quadruplex higher-order structures (G4), in which guanine bases form stacked planar G-quartets stabilised by Hoogsteen hydrogen bonding and cation coordination.[1] Bioinformatics analyses of the human genome have revealed an elevated frequency in the occurrence of these sequences, notably in telomeres and promoter regions of genes such as the oncogenes *c-Myc*, *c-Kit*, and *K-Ras*,[2] thus suggesting that G4s may naturally act as regulatory elements, particularly in cell proliferation processes.[3] Recently, the 27-nucleotide sequence located 77 nucleotides upstream of the transcription start site of *Hsp90*, a gene that encodes a protein involved in the regulation of cell proliferation and a validated target for cancer therapy,[4] was also shown to form stable quadruplex DNA structures.[5] Down-regulation of transcription by small molecules that are able to induce and stabilise DNA G4 structures has been reported for oncogenes *c-Myc*,[6] *c-Kit*,[7] *KRas*,[8] and *Hsp90*,[9] reinforcing the concept that G4s are promising targets for the design of new compounds (G4 ligands) with potentially high cancer cell selectivity and lower toxicity than standard DNA-targeting anticancer drugs.[3a] Moreover, targeting G-quadruplexes in promoter oncogenes has several advantages over targeting expressed proteins, including the decreased likelihood of point mutations and resistance. However, from a drug-discovery perspective, we are still taking the first steps, as there is currently restricted diversity in the available G4 ligands, and these have low affinity and selectivity for G4 relative to protein inhibitors.[3a] The large planar and aromatic surface of a terminal G-quartet is a common G4 chemical feature that has led to the development of mainly three G4 ligand families: the macrocyclic family, of which the porphyrin derivative TMPyP4 and telomestatin are well-known examples; the polyaromatic fused family, which includes acridines, anthra-

[a] Dr. J. Lavrado, Prof. R. Moreira, Dr. D. J. V. A. d. . Santos, Dr. A. Paulo
Medicinal Chemistry Group
Research Institute for Medicines and Pharmaceutical Sciences
Faculty of Pharmacy, University of Lisbon
Av. Prof. Gama Pinto, 1649-003 Lisbon (Portugal)
E-mail: mapaulo@ff.ul.pt

[b] Dr. P. M. Borralho, Dr. R. E. Castro, Prof. C. M. P. Rodrigues
Molecular & Cell Biology of Eukaryotic Systems Group
Research Institute for Medicines and Pharmaceutical Sciences
Faculty of Pharmacy, University of Lisbon
Av. Prof. Gama Pinto, 1649-003 Lisbon (Portugal)

[c] Dr. P. M. Borralho, Dr. R. E. Castro, Prof. C. M. P. Rodrigues
Department of Biochemistry and Human Biology
Faculty of Pharmacy, University of Lisbon
Av. Prof. Gama Pinto, 1649-003 Lisbon (Portugal)

[d] Dr. S. A. Ohnmacht, Prof. S. Neidle
The School of Pharmacy, University College London
29/39 Brunswick Square, London WC1N 1AX (UK)

[e] Dr. D. J. V. A. d. . Santos
REQUIMTE, Department of Chemistry & Biochemistry
Faculty of Sciences, University of Porto
R. do Campo Alegre, 4169-007 Porto (Portugal)

Supporting information for this article is available on the WWW under http://dx.doi.org/10.1002/cmdc.201300288.

quinones, and indoloquinoline derivatives; and the family of aromatic non-fused systems such as 1,4-triazole derivatives.[10] Many of these G-quadruplex ligands are selective for G4 structures over duplex DNA, but the design of inter-G4 selective ligands remains challenging. However, in view of the high number of putative G4-forming sequences revealed by the analysis of the human genome, this issue needs to be addressed in order to avoid secondary and undesirable effects in any therapeutic application of G4 targeting. Monomolecular G4s can adopt a wide diversity of topologies and have various loops, grooves, and capping structures as a consequence of differences in their primary DNA sequences. Adenines, thymines, and phosphate groups present in loops, grooves, and capping structures of G4 provide distinct patterns of hydrogen bonding, hydrophobic π surfaces, and negative charges that can be selectively targeted.[11] Crystallographic and NMR studies of G4–ligand complexes have shown that fused polyaromatic ligands such as acridines and indoloquinolines bind to G4s through π–π stacking with guanines of terminal G-quartets, while side chains target the grooves and loops of the G4, contributing both to enhanced binding and selectivity between G4s.[12]

Indoloquinolines are tetracyclic aromatic alkaloids with high potential to be developed into anticancer drugs, but have been insufficiently exploited.[13a] Derivatives of natural indolo[3,2-*b*]quinolines **1** (quindoline) and **2a** (cryptolepine) were previously shown to be good G4 ligands, telomerase inhibitors, oncogene (*c-Myc*) transcription inhibitors, and are able to induce cell-growth arrest (Figure 1).[14] Moreover, the drug-like

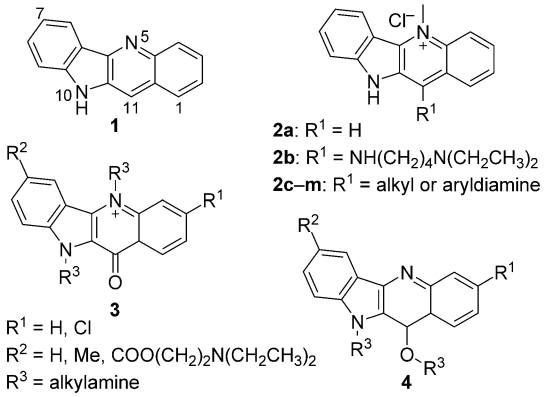

Figure 1. Quindoline (**1**), cryptolepine (**2a**), C11 derivatives **2b**–**m**, and quindoline derivatives **3** and **4** screened against a small panel of G-quadruplexes.

analogue NSC748393 (**2b**) showed good in vitro and in vivo anticancer profiles, as well as strong binding affinity to a telomeric G-quadruplex.[15] However, as for most G-quadruplex ligands known to date, C11-substituted or N10,C11-disubstituted indolo[3,2-*b*]quinolines are poorly selective G4 ligands.[14b,15] Nevertheless, the asymmetric shape of the indolo[3,2-*b*]quinoline aromatic core and the substantial derivatisation potential offered by this structure suggest that it is a very appropriate scaffold for exploitation to obtain efficient and selective G4 ligands.

Embracing the challenge of expanding the chemical toolbox of effective G4 ligands for cancer therapy, herein we describe the design, synthesis, and G4 thermal stabilisation effects of a set of mono-, di-, and trisubstituted indolo[3,2-*b*]quinolines against three different DNA sequences—F21T human telomeric quadruplex (F21T), *c-Kit2*, and *Hsp90A* quadruplexes—using a high-throughput fluorescence resonance energy transfer (FRET) melting assay. Molecular modelling was then used to rationalise the binding to telomeric quadruplexes, and the antiproliferative activity of the most effective and selective ligands were evaluated in cancer and normal cells.

Results and Discussion

Design of target compounds

Previous studies have shown that thermal stabilisation of telomeric or *c-Myc* G4 by quindoline (**1**) derivatives increases with increasing basicity of the quinoline nitrogen (N5) atom, for example, when an electron-donating group (NH) is present at C11.[14b] These results have been interpreted as indicating that a positive charge near the aromatic core, due to protonation of N5 at physiological pH, is an important feature to improve binding to external G-quartets of G4 DNA structures.[14a,b] Methylation of N5, leading to a stable positive charge, further increased binding affinity and thermal stability of telomeric G4, an effect that was ascribed to increased π–π stacking interactions, due to a decrease in electron density in the aromatic core.[14c] As reported for other G4 ligands, the basicity of the quindoline side chains is also important for G4 binding,[14c] but other chemical features of basic side chains remain unexploited. In this context, we first decided to expand the chemical diversity of the basic side chain at C11 and to evaluate the effect of N5-methyl quindoline derivatives **2c**–**m**, containing various alkyl side chain lengths, terminal amine groups (primary, secondary, or tertiary), and different aryl side chains on G4 thermal stabilisation.

It has been reported that appending two basic side chains to C2 and C7 or N10 and C11 of the quindoline core increases binding to telomeric[16] or *c-Myc* G4 structures.[14b] Because no other positions of the asymmetrical quindoline nucleus have been exploited to modulate G4 binding, we next designed new indolo[3,2-*b*]quinolines, **3** and **4**, with two and three basic side chains, to evaluate the effect of various alkylamine substitution patterns and of substituents at positions 3 and 7 on interactions with different G4 structures.

Chemistry

Indolo[3,2-*b*]quinolines **2**–**4** were synthesised via quindolones **8** (indolo[3,2-*b*]quinolin-11-ones), according to the route illustrated in Scheme 1 and based on a procedure developed by Görlitzer and Weber and adapted by Bierer.[13] In the first step anthranilic acids **5** were allowed to react with bromoacetyl bromide to afford compounds **6**, which were then converted into the corresponding 2-(2-(phenylamino)acetyl)benzoic acids **7** by reaction with the appropriate aniline. Acid-promoted bi-

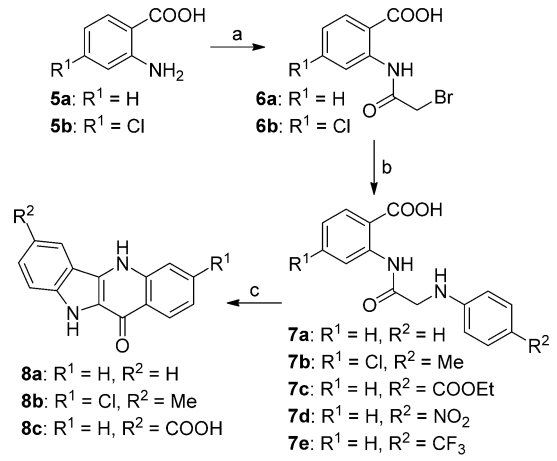

Scheme 1. Synthesis of the indolo[3,2-*b*]quinoline nucleus. *Reagents and conditions*: a) bromoacetyl bromide, DMF/1,4-dioxane (1:1), RT, overnight; b) appropriate aniline; c) PPA, 130 °C, 2 h.

cyclisation of **7a–c** with polyphosphoric acid (PPA) afforded the corresponding quindolones **8a–c**. However, PPA-promoted cyclisation of **7d** did not afford the corresponding quindolone (R^1 = H, R^2 = NO_2), but another unexpected compound. The ^{1}H NMR spectra and ^{1}H–^{1}H COSY data showed a total of eight protons, instead of seven protons, and two inter-correlated sets of doublets integrating for two protons each at 6.56 and 7.52 ppm, as in **7d** for the 4-nitroaniline ring. The total assignment of the ^{1}H and ^{13}C NMR chemical shifts by analysis of 2D HMQC and HMBC allowed the identification of 2-hydroxy-3-((4-nitrophenyl)amino)quinolin-4(1*H*)-one (**7id**) as the product of PPA-catalysed cyclisation of **7d**. This observation led us to propose the two-step mechanism depicted in Scheme 2. In the case of **7d**, bearing a *para*-nitro group in the aniline moiety, the indoloquinoline cyclisation reaction stopped after the closure of the six-membered ring, possibly due to the strong electron-withdrawing effect of the nitro substituent which precluded closure of the five-membered ring and formation of the final quindolone.

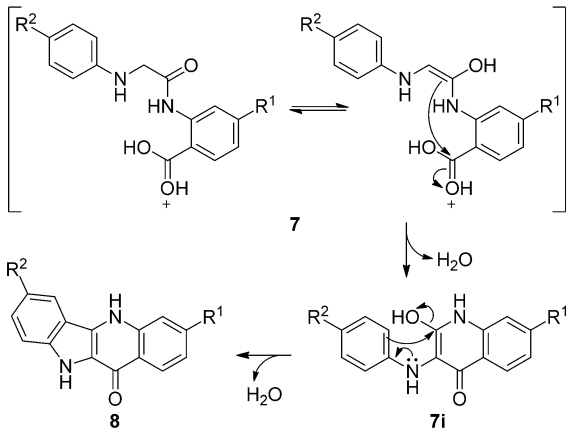

Scheme 2. Acid-promoted cyclisation mechanism of **7** to afford quindolones **8**.

In addition, acid-promoted bicyclisation of **7e**, with a trifluoromethyl substituent, gave quindolone **8c**, with a carboxylic acid group, as a bicyclisation product of **7c**. Compound **8c** was fully characterised by NMR spectroscopy, which revealed two carbonyl carbons in the ^{13}C spectra at 167.92 and 168.18 ppm. The carbon at 168.18 ppm showed a ^{1}H–^{13}C HMBC correlation with the singlet resonating at 8.99 ppm assigned to the proton at position 6 of the aromatic nucleus. Analysis of the 2D NMR spectra allowed assignment of the remaining carbonyl signal to C11 of the aromatic nucleus. Furthermore, ^{19}F NMR data of the product from **7e** bicyclisation did not reveal any signal resonating in the spectrum, in contrast to what was observed for the starting material **7e**, which showed a singlet at −59.09 ppm. Mass spectrometric analysis also corroborates the presence of a carboxylic acid instead of a trifluoromethyl substituent. In this particular system, the electronic effect of the indole nitrogen atom promoted an S_N1-type cleavage of the C–F bond in the trifluoromethyl group, as described for 3-(trifluoromethyl)-1*H*-indoles, followed by hydrolysis of the difluoromethylene intermediate.[17]

Cryptolepine (**2a**) and derivatives **2c–m** were obtained from **8a** after 11-chlorination with phosphorus oxychloride. Hydrogenation and N5-methylation with methyl trifluoromethanesulfonate gave **1** and N5-methylation of the 11-chloro intermediate, followed by nucleophilic substitution with the required alkyldiamine to yield **2c–m**. All cryptolepine derivatives were fully characterised by NMR, and in all cases, purities were ≥95 %, as described elsewhere.[18] Quindoline derivatives **3** and **4** were obtained by reaction of **8** with the appropriate chloroalkylamine in the presence of a base, as described in a synthetic procedure recently reported by our group (Scheme 3).[19] In the case of the intermediate quindolone **8c**, the same synthetic procedure afforded the trialkylated derivatives **3d** and

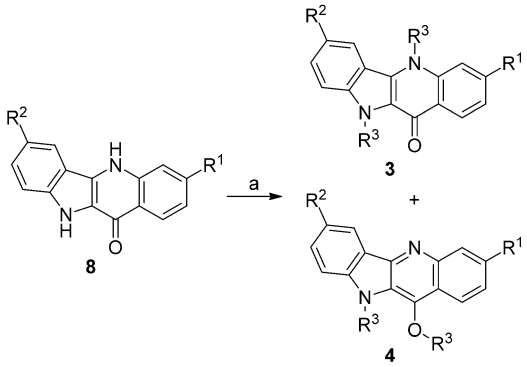

Scheme 3. Synthesis of indolo[3,2-*b*]quinoline derivatives **3** and **4**. *Reagents and conditions*: a) chloroalkylamine, K_2CO_3, dry acetone, reflux, overnight.

4d. The positions of *N*-alkylamine side chains in compounds **3a–d** and **4a–d** were assigned on the basis of ^{1}H–^{13}C correlations between CH_2 protons of the side chain and quaternary carbon atoms of the quindoline aromatic structure, observed in HMBC spectra and confirmed by NOE experiments. For example, ^{1}H and ^{13}C spectra of derivative **4d** displayed signals

corresponding to the introduction of three side chains in the quindoline nucleus. The disappearance of the carbonyl carbon signal resonating at 167.92 ppm in **8c** (C11), replaced by a typical phenoxy carbon signal at 145.15 ppm and an additional ether carbon (74.79 ppm), correlating in the HMQC with a ^{1}H triplet (4.31 ppm), indicated the presence of an alkoxy chain at C11.

This triplet revealed a NOE correlation with a triplet at 4.73 ppm, which correlated in HMBC with C9a and C10a (147.36 and 125.30 ppm, respectively) and in the ^{1}H–^{1}H COSY spectrum with two methylene protons, corroborating the introduction of a second side chain at position N10. The third side chain was characterised in ^{1}H NMR data by two triplets, integrating to two protons each, at 2.96 and 4.49 ppm, one quartet at 2.70 ppm integrating for four protons, and one triplet at 1.12 ppm integrating for six protons. The triplet at 4.49 ppm correlated in the HMBC spectrum with the carbonyl carbon (166.84 ppm), which in turn correlated with the singlet at 9.24 ppm, assigned to H6, thus confirming the introduction of the third side chain in the carboxylic acid moiety of **8c** and formation of the 2-(diethylamino)ethyl-11-[2-(diethylamino)-ethoxy]-10-[2-(diethylamino)ethyl]-10*H*-indolo[3,2-*b*]quinolone-7-carboxylate (**4d**) (Supporting Information).

G-quadruplex stabilisation

The ability of the indolo[3,2-*b*]quinolines **2**–**4** to bind and stabilise G4 structures and a self-complementary hairpin DNA (T-loop) was evaluated by FRET melting assays with ligand concentrations ranging from 0.1 to 5 μM. The FRET melting data, given as changes in melting temperature (ΔT_m) and obtained with fluorescently labelled DNA G4 sequences (0.2 μM) of F21T human telomeric DNA[20] and of oncogene promoter sequences *c-Kit2*[7a] and *Hsp90A*,[5] as well as with T-loop in potassium ion buffer, are summarised in Tables 1 and 2. The results show that the indolo[3,2-*b*]quinolines **2**–**4** produce a wide range of G4 stabilisation effects, and, for all compounds, these effects are concentration dependent, with much higher stabilisation effects at 5 μM than at 1 μM, as shown in Figure 2 for **2e** and **4d** (see Supporting Information for the remaining compounds).

Cryptolepine derivatives **2c**–**m** showed ΔT_m values ranging from 2 to 25 °C at 2 μM for *Hsp90A*, F21T, and *c-Kit2*, in most cases increased relative to parent compound **2a** and are similar to those reported elsewhere for human telomeric G4.[14c,15] Compounds with aliphatic amine side chains (**2c**–**i**), which at physiological pH are expected to be double protonated,[21] showed higher stabilisation effects with G4. From those, **2e**–**g** with propyl side chains showed the highest degree of stabilisation, with ΔT_m values ranging from 17 to 25 °C. These results show for the first time in the case of C11-monosubstituted indolo[3,2-*b*]quinolines, that there is an optimal NH-alkylamine side chain length for G4 stabilisation, in accordance with previous observations for di- and trisubstituted acridines[22] and naphthalene diimides,[23] that propylamine side chains are superior to ethyl or butylamine. Changing the distal part of the propylamine side chain from a primary to a secondary or tertiary amine (**2e**–**g**) does not significantly change the complex stabilisation, despite the differences between pK_a values observed for those amine groups (pK_a values ranging from 8.7 to ~12).[21] However, compound **2d**, which contains a weak terminal amine with a pK_a value of 7.7,[21] or compound **2l** with an *N*-(2-hydroxybenzyl)piperidine side chain in which the basicity of the tertiary amine is expected to be lower due to hydrogen bond interactions with the 2-hydroxy group of benzyl, and compounds **2j**,**k**,**m** that have no basic side chains, showed lower G4 stabilisation (ΔT_m: 2–15 °C). This confirms that electrostatic or hydrogen bond interactions between the ligand protonated side chain and the G4 structures are important factors for complex stabilisation, as suggested by molecular modelling studies,[14c] although this could not be confirmed by NMR analysis of a *c-Myc* promoter G4 and the 11-((2-dimethylamino)ethylamino)quindoline complex.[12c] The melting data for T-loop with compounds **2** showed, in most cases, a similar outline in comparison with G4 data (Table 1), and no significant selectivity for G4 structures would be expected.

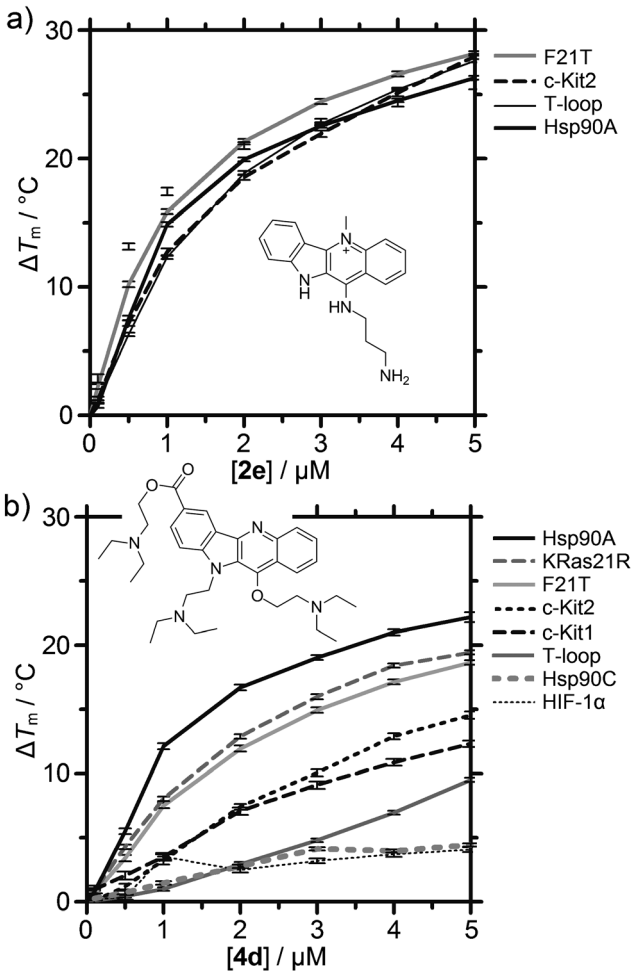

Figure 2. Concentration-dependent FRET melting profile of G4 structures and T-loop DNA complexed with compounds a) **2e** and b) **4d**.

The indolo[3,2-*b*]quinolines with two (**3a**–**c**, **4a**–**c**) and three (**3d**, **4d**) alkylamine side chains, which are expected to be di- and triprotonated at physiological pH, respectively, were found

Table 1. Melting temperatures of DNA structures stabilised by **2a–m** at 2 μM.

Compd	R^1	ΔT_m [°C][a]			
		Hsp90A[b]	F21T[c]	c-Kit2[d]	T-loop[e]
2a	H	10.1	7.0	5.0	3.2
2c	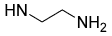	18.7	13.9	12.3	7.8
2d	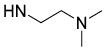	12.1	11.4	8.1	9.3
2e	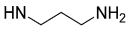	19.9	21.3	18.6	18.9
2f	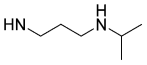	25.0	21.9	16.8	19.3
2g	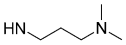	23.8	21.3	17.0	19.9
2h	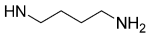	22.2	18.4	13.5	13.9
2i	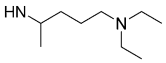	18.0	15.8	11.4	14.5
2j		9.6	5.5	2.78	4.7
2k		9.8	5.9	3.5	3.5
2l	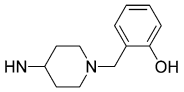	15.6	10.9	7.5	6.4
2m		6.8	3.0	2.1	1.5

[a] $\Delta T_m \pm 0.3$. [b] $T_m = 59.0$ °C. [c] $T_m = 57.9$ °C. [d] $T_m = 58.4$ °C. [e] $T_m = 53.2$ °C.

to be less effective stabilisers of G4 structures ($\Delta T_m < 17$ °C) than monosubstituted N5-methylindoloquinolines **2c–i**. This observation suggests that the positive charge at the aromatic moiety, which can be ascribed to decreased electron density and consequently stronger interactions with the electron-rich π system of a G-quartet, is more important for G4 stabilisation than positive charges at side chain termini, as in the case of **3** and **4**. This is consistent with the type of interactions observed between 11-((2-dimethylamino)ethylamino)quindoline and the *c-Myc* G4 complex studied by NMR.[12c] These studies showed that the principal forces stabilising the complex are π–π stacking between the aromatic indoloquinoline ring of the ligand and two guanines of the terminal G-quartet, whereas no particular interactions were observed between the side chain and the G4 structure, although this could be due to the short side chain length of the ligand.

Generally, N5,N10-disubstituted indolo[3,2-*b*]quinolines **3a–c** showed greater G4 stabilisation, and in particular **3b** with a propylamine side chain (ΔT_m between 12 and 7 °C), than the counterparts **4a–c** (ΔT_m of **4b** between 5 and 3 °C), with both side chains close to each other (at N10 and C11) and directed to the same side of the indolo[3,2-*b*]quinoline aromatic core. Boddupally et al.[14b] recently reported that the introduction of a second alkylamine chain at N10 of an 11-piperazinylquindoline increases the thermal stability of a *c-Myc* G4 complex, although subsequent competition dialysis experiments showed that monosubstituted 11-piperazinylquindoline has higher binding affinity for G4 structures than the corresponding N10,C11-disubstituted compound. Remarkably, competition dialysis experiments also showed that despite the lower binding affinity for G4 structures, disubstituted quindolines bind more selectively to different G4 than monosubstituted compounds,[14b] a pattern also observed in this study. N5,N10-disubstituted indoloquinolines **3a–b** show a G4 thermal stability trend effect of *Hsp90A* > F21T > *c-Kit2*. Also, ΔT_m values for T-loop suggest a weak binding affinity for duplex DNA structures. Finally, to our surprise, the introduction of an electron-withdrawing chlorine atom at the 3-position of the indolo[3,2-*b*]quinoline aromatic core seems to decrease the G4 binding capacity of the N5,N10-disubstituted compound, as **3c** has a lower ΔT_m (5 °C for *Hsp90A* and 2 °C for F21T) than the ethyl side chain analogue **3a** (ΔT_m values of 8 °C for *Hsp90A* and 4 °C for F21T).

The introduction of an alkylamine carboxylate side chain at the 7-position of the indolo[3,2-*b*]quinoline aromatic core, as in the case of trisubstituted compounds **3d** and **4d**, clearly improves binding to G4 DNA structures (ΔT_m between 16 and 7 °C for both compounds), maintaining the inter-G4 thermal stability trend effect *Hsp90A* > F21T > *c-Kit2* > T-loop (see Figure 2b for compound **4d**) and also suggesting weak binding affinity for duplex DNA structures. However, in the case of trisubstituted indoloquinolines **3d** (C7,N5,N10-substituted) and **4d** (C7,N10,O11-substituted) the relative positions of the three side chains has no effect on G4 stabilisation, as observed for disubstituted indoloquinolines **3a–c** (N5,N10-substituted) and **4a–c** (N10,O11-substituted). Overall, the results suggest that the electron-withdrawing carboxylate group at the 7-position can increase π–π stacking interactions between the aromatic indoloquinoline ring and the terminal G-quartet of G4s by decreasing the electron density of the former.

The trisubstituted derivatives **3d** and **4d** were also evaluated for their stabilisation effects on the G4-forming promoter sequence of *KRas*[24] (Table 2). Compound **4d** is as good a stabiliser of the G4 sequence *KRas21R* ($\Delta T_m = 13$ °C) as of F21T. The G4 stabilising effect of compound **4d** was further evaluated with *c-Kit1*,[7a] *HIF-1α*,[25] and *Hsp90C* (comprising the full G4 sequence in the *Hsp90* promoter region)[5] (Figure 2). The results showed a similar stabilisation of the oncogenic *c-Kit1* G4 ($\Delta T_m = 7$ °C at 2 μM ligand concentration), compared with *c-Kit2* and lower stabilisation of *HIF-1α* ($\Delta T_m = 3$ °C) relative to the remaining G4 structures. Despite **4d** being a good stabiliser of *Hsp90A* G4 ($\Delta T_m = 17$ °C), no significant stabilisation of the oncogene promoter *Hsp90* full sequence G4 was observed ($\Delta T_m = 3$ °C). These results further suggest the capacity of trisubstituted indolo[3,2-*b*]quinolines to discriminate between G4 structures.

To access the selectivity of these ligands for G4 over duplex DNA, suggested by ΔT_m data, competitive FRET experiment with F21T G4 and **4d** was performed in the presence of a non-fluorescent duplex DNA competitor (26ds)[26] (Figure 3). The results indicate that stabilisation of the telomeric G4 is only affected in the presence of 50-fold excess of competitor 26ds, showing that this compound is at least 10-fold more selective for G4 than for duplex DNA.

Table 2. ΔT_m values of DNA structures stabilised by compounds **3** and **4** at 2 μM and ΔG values of the optimised propeller-like parallel (1KF1), antiparallel basket-type (143D), hybrid-type 1 (2HY9), and hybrid-type 2 (2JPZ) G4 structures with compounds **3** and **4**.

Compd	R^1	R^2	R^3	ΔT_m [°C][a]					ΔG [kcal mol^{-1}]			
				Hsp90A[b]	F21T[c]	c-Kit2[d]	T-loop[e]	KRas21R[f]	1KF1	143D	2HY9	2JPZ
3a	H	H		7.6	3.8	2.3	0.5	ND	−42.7	−45.4	−65.1	−67.6
3b	H	H	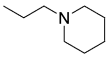	11.8	7.2	7.5	3.8	ND	−43.9	−40.6	−71.6	−67.9
3c	Cl	CH_3		5.0	1.7	1.4	0.5	ND	−43.3	−35.7	−67.6	−68.7
3d	H	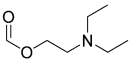		15.9	10.6	8.7	2.2	7.4	−44.7	−38.1	−72.6	−83.6
4a	H	H		3.2	1.2	1.1	1.8	ND	−40.5	−36.0	−53.8	−63.9
4b	H	H	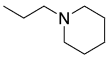	5.2	2.5	2.4	2.2	ND	−42.5	−43.0	−68.5	−64.0
4c	Cl	CH_3		3.2	1.4	0.9	0.3	ND	−40.4	−34.2	−60.2	−62.2
4d[g]	H	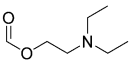		16.7	12.0	7.4	2.9	12.9	−50.0	−40.2	−73.5	−77.6

[a] $\Delta T_m \pm 0.3$. [b] $T_m = 59.0$ °C. [c] $T_m = 57.9$ °C. [d] $T_m = 58.4$ °C. [e] $T_m = 53.2$ °C. [f] $T_m = 51.5$ °C; ND: not determined. [g] Also evaluated with: c-Kit1 ($T_m = 60.2$ °C), $\Delta T_m = 7.1 \pm 0.3$ °C; Hsp90C ($T_m = 78.5$ °C), $\Delta T_m = 2.8 \pm 0.1$ °C; HIF-1α ($T_m = 79.5$ °C), $\Delta T_m = 2.5 \pm 0.2$ °C.

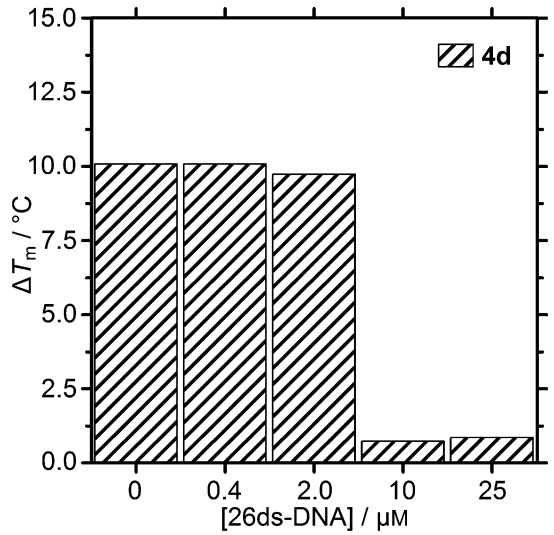

Figure 3. FRET melting competition assay data for the F21T–**4d** complex in the absence (0 μM) and presence of increasing concentrations of duplex (26ds) DNA competitor; the concentration of F21T was 0.2 μM.

Molecular modelling studies

To understand the structural basis of G4 binding in this class of ligands, molecular modelling of several compounds with available G-quadruplexes structures was performed. Based on FRET melting data, which showed the highest stabilisation of G4 structures in the promoter of *Hsp90A* and human telomeres by indolo[3,2-*b*]quinolines, and in the absence of *Hsp90A* G4 structure, several intramolecular G4 structures with different topologies were selected.[27]

In physiologically relevant potassium ion concentrations, human telomeric DNA can adopt antiparallel, hybrid, or parallel arrangements.[28] However, due to water depletion, the antiparallel and hybrid arrangements under crowded conditions are converted into propeller-type parallel strands.[29] To generate our models, four experimentally determined structures of G4 human telomere were chosen as starting points: 1) the 22-mer unimolecular propeller-like parallel with three stacked G-quartets (PDB ID 1KF1);[30] 2) the 22-mer unimolecular antiparallel basket-type with three stacked G-quartets, which are connected by two lateral loops and a central diagonal loop (PDB ID 143D);[31] and 3) and 4) the 26-mer unimolecular hybrid-type 1 and -type 2 mixed parallel/antiparallel-G-stranded G-quadruplexes (PDB IDs 2HY9 and 2JPZ, respectively).[32]

To achieve the 21-mer common sequence 5′-GGG TTA GGG TTA GGG TTA GGG-3′ in all topologies, in PDB 1KF1 and 143D, the nucleotide 5′-A was removed, nucleotides 5′-AAA and AA-3′ were removed in PDB 2HY9, while nucleotides 5′-TTA and TT-3′ were removed in PDB 2JPZ. The presence of the K^+ ions are very important for the stability of G4; the absence of coordination cations modifies the structures, causing evident deformation or disruption.[33] Therefore, K^+ ions were added between the guanine stacks to the first single G4 of the ensembles of NMR structures (PDB IDs 143D, 2HY9, and 2JPZ) and used as starting points. Refinement of the G4 structures was performed by molecular dynamics (MD) simulations in water with the appropriate number of counterions for neutrality of the system and sampling the *NpT* ensemble ($p = 1$ bar, $T = 298$ K) for 10 ns. During the complete course of MD simulation the integrity of the G4 persisted, with the RMSD of all atoms of the structure stabilising around 1.9, 2.5, 2.6, and 2.5 Å for

parallel, antiparallel, hybrid-type 1, and -type 2, respectively (Supporting Information). The stacked G-quartets are very rigid and are the most stable segment of the structure due to strong hydrogen bonds and stacking interactions. However, without impact on the structure of the central G-tetrad core, the residue's root-mean-square fluctuation (RMSF) showed that loop nucleotides exhibited relatively larger flexibility, (Supporting Information), as recently described by Haider and co-workers for the human propeller telomeric DNA quadruplex.[34] To evaluate indolo[3,2-*b*]quinoline complex formation with the optimised structures, several docking studies were performed using the MD-optimised G4 structures with different topologies as starting conformations. The efficiency of the docking methodology was validated with the crystal structure of the human telomeric bimolecular parallel-stranded G4, co-crystallised with the acridine BRACO-19 (PDB ID 3CE5),[12b] using rigid- and induced-fit docking protocols and several refinement scoring functions included in MOE v.2012.10.[35] The final docking pose obtained with rigid docking protocol and alpha HB scoring function was in good agreement with the crystallographic pose in the 3′ end of structure, showing an RMSD of 1.8 Å for all heavy atoms, demonstrating the effectiveness of the chosen methodology (Supporting Information).

Docking studies of the indolo[3,2-*b*]quinoline derivatives **3** and **4** were performed with the different topologies of the 21-mer human telomere G4. The final docking poses showed **3** and **4** interacting with the propeller-like parallel, hybrid-type 1 and -type 2 models in a stacking mode on the top of the 3′ G-quartet, while in the anti-parallel basket-type model, the ligands behave like groove binders due to the steric hindrance caused by the TTA loop (Supporting Information). The free energy of complex formation (ΔG) was estimated from the final docking poses after energy refinement (Table 2). The highest stabilisers of the human telomere F21T G4 structure, **3d** and **4d**, showed to be the most favourable predicted stabilisers, with the lowest ΔG values, as reported elsewhere for quindolines and fluorenone derivatives.[14c,36] Coefficients of determination (r^2) of 0.74, 0.65, and 0.80 (Supporting Information) were found between the F21T FRET data and ΔG for **3** and **4** with the propeller-type parallel, hydrid-type 1 and -type 2 models, respectively. Analysis of ΔG values showed the most stable binding modes converging to the hydrid-type 2 human telomere G4 topology, possibly indicative of the most favourable conformation in our experimental assays.

Our studies showed that for the propeller-like parallel structure (1KF1), the N5,N10-indolo[3,2-*b*]quinolines **3a–c** stack at the centre of the G-quartet. The complex is stabilised by asymmetrical π–π stacking interactions, and, in some cases, with the side chains extended over the G-quartet face, stabilised via a π–cation interaction between protonated terminal nitrogen and a guanine base. On the other hand, N5,O11 derivatives **4a–c** also showed stacking interactions with the guanine bases of propeller-like parallel G4, but due to a less favourable conformation, both side chains point toward the outside of the G4, leading to decreased stabilisation, as shown by higher ΔG values (Table 2). In the hybrid-type 1 and -type 2 topologies, derivatives **3a–c** and **4a–c** stack on the edge of the G-quartet due to steric hindrance caused by the TTA loops. The complex is also stabilised by asymmetric π–π stacking interactions, and in some cases the N10 side chain in **3a–c** also extends over the G-quartet, as in the parallel topology, interacting with guanine or thymine bases. The N5 side chains of **3a–c** point toward the outside of the G-quartet core, able to interact with the TTA loops and/or phosphate backbone and probably justifying the higher stabilisation revealed by the ΔG values in comparison with propeller-type parallel topology. On the other hand, docking results for derivatives **4a–c** in the hybrid-type structures showed both N10 and O11 side chains pointing toward the outside of the G-quartet core, and probably justifying the highest ΔG values when compared with **3a–c**. Generally, unlike in the propeller-type parallel topology, the edge placement of **3** and **4** found in the hybrid-type structures allows interactions between the side chains and the TTA loops and/or backbone, in accord with the higher stabilisation properties predicted by the ΔG values (Table 2) in the latest structures.

As already described, trisubstituted derivatives **3d** and **4d** showed higher stabilising properties (ΔT_m and ΔG) than disubstituted derivatives; therefore, the influence of a third aminoalkylcarboxylate side chain at position 7 was also modelled. Compounds **3d** and **4d** were docked against the four different G4 topological structures. Docking results in the propeller-like parallel structure showed derivatives **3d** and **4d** interacting with the G-quadruplex structure as already described for **3a–c** and **4a–c**, yet with the third side chain at position 7 acting as a new anchoring point. In both cases, the C7 side chain is directed outside the G-quartet core, allowing interactions with the external loops and/or backbone of the G4 structure and justifying the increased experimental and predicted binding properties (ΔT_m and ΔG), when compared with the disubstituted derivatives. In the hybrid-type G4 structures, **3d** and **4d** showed the same asymmetric π–π stacking interactions of the indolo[3,2-*b*]quinoline nucleus with two guanine bases, on the edge of the G-quartet. For instance, Figure 4 shows the top-ranked docking pose for **4d** in the hybrid-type 2 human telomere G4 structure.

The complex is stabilised by asymmetric π–π stacking interactions between the indole ring and guanine DG4. Additionally, hydrogen bond interactions between the O11 terminal nitrogen and the phosphate backbone, and between the protonated C7 terminal nitrogen and N3 of the guanine DG12 purine ring improve complex stability. As described for the propeller-type parallel structure, in the hybrid-type structures, the third side chain in C7 adds an additional point of contact with G4, improving the stability of the complex. As such, this additional binding feature described for **3d** and **4d** is probably correlated with the generalised increase in binding predicted by the ΔG values, and is in accord with the ΔT_m values found for the trisubstituted derivatives for all the G4 structures evaluated.

Effect on HCT116 cancer cells

To examine the effect of G4-selective ligands **3d** and **4d** on cancer cells, the antiproliferative activity of these compounds

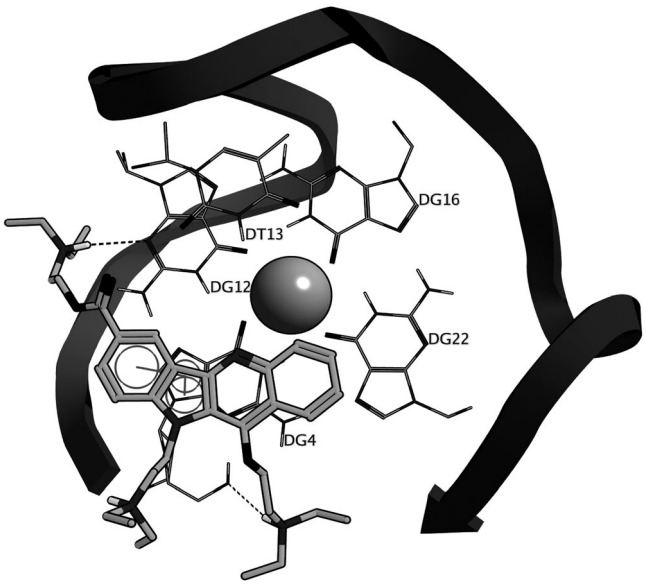

Figure 4. Top view of the predicted pose, upon docking with MOE, of compound **4d** and the optimised 21-mer hybrid-type 2 G4 structure (PDB ID 2JPZ). The G4 structure is represented as a wireframe and the ligand as sticks. Non-relevant bases and nonpolar hydrogen atoms were removed for clarity; grey lines represent π interactions, and black dashed lines indicate hydrogen bond interactions.

was evaluated by means of MTS assays with the HCT116 colon cancer cell line after drug exposure for 96 h. HCT116 cells were selected, as these cells overexpress Hsp90 and KRas proteins. We also evaluated the selectivity of **3d** and **4d** for cancer cells by assessing the effect of these compounds on the viability of primary rat hepatocytes. Figure 5 clearly shows that compounds **3d** and **4d** are ~100-fold more selective for HCT116 cells ($IC_{50} = 4.5 \pm 0.6$ and 5.7 ± 0.7 μM for **3d** and **4d**, respectively) than for normal hepatocytes ($IC_{50} > 100$ μM), a pattern also observed for the standard cytotoxic drug used for colon cancer treatment, 5-fluorouracil (5-FU).

However, 5-FU shows a distinct anti-proliferative profile relative to that of G4 ligands **3d** and **4d** over HCT116 human colon cancer cells. Although 5-FU seems to be more effective against HCT116 cancer cells at lower concentrations, its maximum effect is only of 75% cancer cell growth inhibition, even at 100 μM, whereas **3d** and **4d** are more effective, almost completely inhibiting the growth of HTC116 colon cancer cells at low-micromolar concentrations ($IC_{90} = 7.6 \pm 0.9$ and 11.0 ± 0.9 μM for **3d** and **4d**, respectively). The antiproliferative activities of **3d** and **4d** compare with those of other disubstituted indolo[3,2-*b*]quinolines.[14b] We also found that HCT116 cell line exposure to **3d** and **4d** for 72 h decreased the expression levels of Hsp90 and KRas proteins (Figure 6).

Conclusions

Targeting G4 DNA structures at telomeres and promoter regions of oncogenes may be an effective strategy to control cancer cell proliferation, but to date, knowledge of the chemical requirements for both G4 structures and ligands that

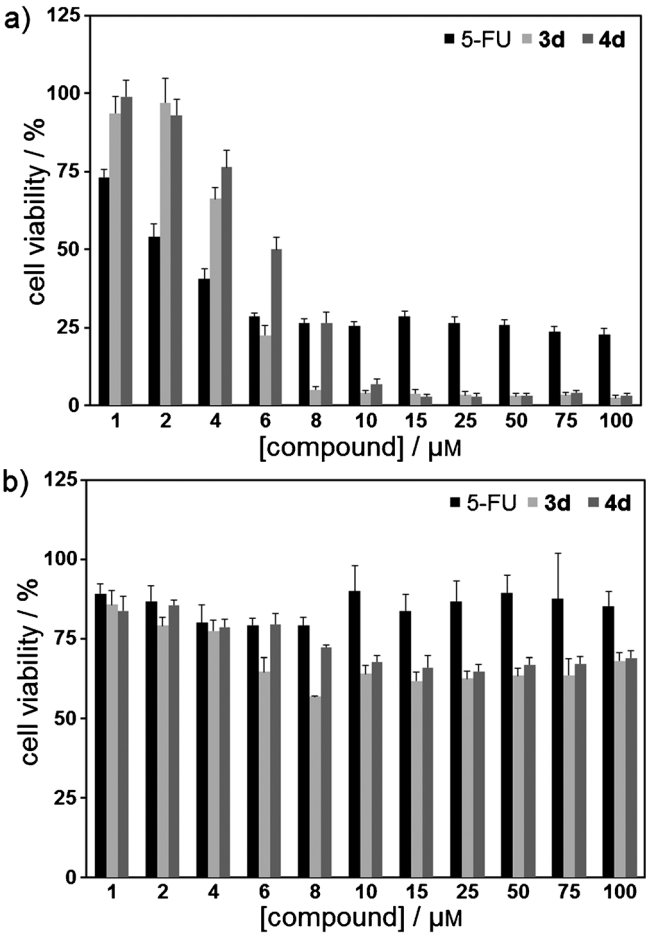

Figure 5. Dose–response curves for a) HCT116 cancer cells and b) primary rat hepatocytes exposure to **3d**, **4d**, and 5-fluorouracil (5-FU).

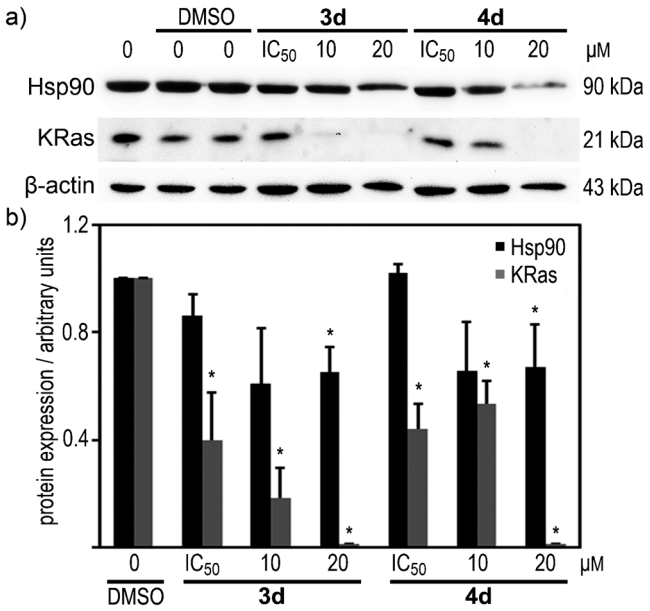

Figure 6. Exposure to compounds **3d** and **4d** decreases Hsp90 and KRas protein expression in HCT116 cells. Total proteins were extracted from HCT116 cells following exposure to **3d**, **4d**, or vehicle (DMSO) for 72 h and used to evaluate Hsp90 and KRas steady-state levels by Western blot. Results are expressed as the mean ± SEM; $^*p < 0.05$ relative to DMSO control.

would lead to high and selective stabilisation of G4 DNA structures is still sparse. To further explore and understand the G4-structure stabilising activity relationship of indolo[3,2-*b*]quinolines, several mono- (**2**), di- (**3a**–**c**, **4a**–**c**), and trialkylamine (**3d** and **4d**) derivatives were designed, synthesised, and evaluated for thermal stabilisation of three different G4 DNA sequences and a hairpin duplex DNA sequence. Further molecular modelling studies were performed to better understand the basis of their binding.

Overall, monosubstituted N5-methyl derivatives, bearing a full cationic charge at the quinoline nitrogen (N5) atom and a protonatable amine group at the side chain terminus (compounds **2c**–**i**) are better G4 DNA stabilisers, but seem to be nonselective for G4 DNA structures. Further analysis of FRET melting data obtained for indolo[3,2-*b*]quinolines with one (**2a**–**m**), two (**3a**–**c**, **4a**–**c**), or three (**3d** and **4d**) alkylamine side chains and molecular modelling results for **3a**–**d** and **4a**–**d** has enabled the following SAR conclusions to be made: 1) Optimal linker length between the distal basic centre and the indolo[3,2-*b*]quinoline moiety seems to be that of propyl linear chains, a pattern also observed with the disubstituted derivatives (**3a**–**b**, **4a**–**c**) and which consistently showed lower ΔG values. 2) Aryl substitution at the 11-position has no effect on G4 thermal stabilisation; compounds **2j**–**k** show ΔT_m values similar to that of parent compound **2a**. 3) The basicity of side chains seems to be positively correlated with thermal G4 stabilisation up to pK_a ~8.5, consistent with increased concentration of the protonated species and clearly suggesting that cationic groups are required for active participation in G4 complex stabilisation. Molecular modelling studies have shown that protonated side chains extend over G-quartets and can form hydrogen bonds and electrostatic interactions with the guanine bases as well as with TTA loops and phosphate backbones. 4) The introduction of a third side chain, an alkylaminoalkylcarboxylate (**3d** and **4d**), increases G4 stabilisation relative to disubstituted derivatives, leading to selectivity for G4 over duplex DNA structures and suggests an inter-G4 selectivity trend of *Hsp90A* > F21T ≈ *KRas21R* > *c-Kit2*. 5) The relative position of side chains plays an important role in the thermal stability of G4 DNA structures. N5,N10-disubstituted indolo[3,2-*b*]quinolines **3a**–**c** are modest G4 stabilisers, whereas N10,O11-disubstituted analogues **4a**–**c** showed very poor G4 DNA stabilising effects. 6) A chlorine atom at the 3-position of the indolo[3,2-*b*]quinoline (compound **3c**) is detrimental to G4 DNA complex stabilisation. Analysis of free binding energies obtained from molecular modelling studies clearly corroborates the FRET experimental data. Molecular modelling studies showed that the relative position of the side chain plays an important role in complex stabilisation, in which the N5,N10-disubstituted indolo[3,2-*b*]quinolines **3a**–**c** can participate in more binding interactions with the G-quartet face, due to a more favourable conformation. Additionally, the introduction of a third side chain at position 7 of the aromatic nucleus (compounds **3d** and **4d**) seems to favour the formation of additional hydrogen bonds and electrostatic interactions with the G-quartet and/or TTA loops, and as such, increases complex stabilisation.

From all indoloquinoline derivatives studied, the trisubstituted compounds **3d** and **4d**, bearing a 7-(aminoalkyl)carboxylate side chain are the most promising, showing high G4 thermal stabilisation (ΔT_m between 17 and 8 °C) with an inter-G4 ΔT_m trend of *Hsp90A* > *KRas21R* ≈ F21T > *c-Kit2*, 10-fold selectivity for G4 over duplex DNA, and 100-fold selectivity for the HCT116 cancer cell line (IC_{50} and IC_{90} < 10 μM) over primary rat hepatocytes. Additionally, **3d** and **4d** decreased Hsp90 and KRas expression levels in HCT116 cancer cells. These results are relevant to the future design and synthesis of new 7-carboxylate indoloquinoline derivatives that aim to improve both G4 stabilisation and selectivity between various G4s.

Experimental Section

Chemistry

Chemicals were purchased from Sigma–Aldrich Chemical Co. Ltd. (Spain) and were used without further purification. All compounds were characterised by NMR spectroscopy, recorded on a Bruker Avance 400 spectrometer at 400 (^{1}H) and 100 MHz (^{13}C), with solvent as internal reference. Chemical shifts (δ) are expressed in ppm. Signal splitting patterns are described as singlet (s), doublet (d), triplet (t), quartet (q), quintet (quint) and multiplet (m), or combinations thereof. Coupling constants (J) are given in Hz. The purity of compounds submitted to biological tests was ≥95% in all cases as determined from elemental analysis (C, H, N), carried out by the Elemental Analysis Unit, University of Santiago de Compostela (Spain), on a LECO model CHNS-932 elemental analyser. MS data were recorded using a Micromass Quattro Micro API, Waters, and were obtained by direct infusion on "Full Scan" mode (m/z 60–800); sample ionisation was made in positive and negative electrospray ionisation modes (ESI^+ and ESI^-). Melting points (mp) were determined with a Bock-Monoscop M instrument. Reactions were monitored by thin-layer chromatography (TLC) using coated silica gel plates (Merck, aluminium sheets, silica gel 60 F_{254}) and aluminium oxide matrix plates (Sigma–Aldrich, PET support, F_{254}). Preparative TLC was performed in aluminium oxide 60 F_{254} (VWR, 200×200 mm glass support, F_{254}). Fluorescent-conjugated oligonucleotides were purchased from Eurogentec Ltd. (UK). Fluorescence measurements were made on a DNA Engine Opticon instrument (MJ Research).

General procedure A. 2-(2-Bromoacetamido)benzoic acid (**6a**): A solution of 2-aminobenzoic acid (10.0 g, 72.9 mmol) in DMF (30 mL) and 1,4-dioxane (30 mL) was cooled to 0 °C. Bromoacetyl bromide (8.0 mL, 91.7 mmol, 1.25 equiv) was added dropwise over a 20 min period, keeping the internal temperature between 0 and 5 °C. After the addition was complete, the ice bath was removed, and stirring was continued overnight at room temperature. The reaction mixture was added to H_2O (300 mL), and the light-yellow precipitate which formed was filtered, washed with H_2O, until neutral pH, and then dried to give 18.1 g (96%) of **6a** as a white solid; mp: 162–165 °C. ^{1}H NMR (400 MHz, DMSO): δ = 11.23 (s, NH), 8.06 (d, J = 8.4 Hz, 1H), 7.62 (dd, J = 7.9, 1.4 Hz, 1H), 7.24 (dd, J = 8.4, 7.3 Hz, 1H), 6.82 (dd, J = 7.9, 7.3 Hz, 1H), 3.87 ppm (s, 2H); ^{13}C NMR (100 MHz, DMSO): δ = 169.20, 165.04, 139.92, 134.06, 131.11, 123.45, 119.99, 117.06, 30.65 ppm.

2-(2-Bromoacetamido)-4-chlorobenzoic acid (**6b**): Reaction of 2-amino-4-chlorobenzoic acid (10 g, 58.2 mmol) and bromoacetyl bromide (14.7 g, 6.3 mL, 72.8 mmol, 1.25 equiv) according to general procedure A gave 17.1 g (99%) of **6b** as a light-yellow solid;

mp: 166–168 °C. ^{1}H NMR (400 MHz, DMSO): δ = 11.73 (s, NH), 8.54 (d, J = 2.1 Hz, 1H), 7.98 (d, J = 8.6 Hz, 1H), 7.24 (dd, J = 8.6, 2.1 Hz, 1H), 4.28 ppm (s, 2H); ^{13}C NMR (100 MHz, DMSO): δ = 169.03, 165.92, 141.54, 138.95, 133.26, 123.73, 119.61, 115.91, 30.98 ppm.

General procedure B. Synthesis of 2-[2-(phenylamino)acetamido]benzoic acid (7a): A solution of **6a** (15.0 g, 58.1 mmol) and aniline (19.0 mL, 208.3 mmol, 3.5 equiv) in DMF (30 mL) was heated at 120 °C for 18 h. After cooling, the reaction mixture was poured into ice-water (500 mL), aqueous 5% KOH was added to solubilise the solid product and adjust the solution to pH 10. Then the mixture was washed with CH_2Cl_2 (3×200 mL). The combined CH_2Cl_2 extracts were set aside, and the aqueous layer was acidified to pH 3 with 5% HBr. The precipitate which formed was collected, washed with H_2O, and then dried, yielding 11.0 g (70%) of **7a** as a white solid; mp: 194–197 °C. ^{1}H NMR (400 MHz, DMSO): δ = 11.96 (s, NH), 8.61 (d, J = 8.7 Hz, 1H), 7.83 (d, J = 7.9 Hz, 1H), 7.47 (dd, J = 8.7, 8.0 Hz, 1H), 7.02 (dd, J = 8.0, 7.9 Hz, 1H), 6.98 (d, J = 7.3 Hz, 2H), 6.50 (d, J = 7.7 Hz, 1H), 6.48 (dd, J = 7.7, 7.3 Hz, 2H), 6.39 (s, NH), 3.73 ppm (s, 2H); ^{13}C NMR (100 MHz, CD_3OD): δ = 170.82, 169.01, 148.08, 140.52, 134.03, 131.08, 128.92, 122.60, 119.32, 116.98, 116.12, 112.36, 48.89 ppm.

4-Chloro-2-{2-[(4-methylphenyl)amino]acetamido}benzoic acid (7b): A solution of **6b** (4.0 g, 13.6 mmol) and 4-methylaniline (2.93 g, 27.3 mmol, 2 equiv) in DMF (15 mL) was heated at 120 °C for 48 h and treated according to general procedure B to give 3.68 g (83%) of **7b** as a light-yellow solid; mp: 187–189 °C. ^{1}H NMR (400 MHz, DMSO): δ = 12.13 (s, 1H), 8.83 (d, J = 2.0 Hz, 1H), 7.94 (d, J = 8.5 Hz, 1H), 7.21 (dd, J = 8.5, 2.0 Hz, 1H), 6.91 (d, J = 8.3 Hz, 2H), 6.49 (d, J = 8.3 Hz, 2H), 3.81 (s, 2H), 2.14 ppm (s, 3H); ^{13}C NMR (100 MHz, DMSO): δ = 172.15, 168.74, 146.19, 142.00, 139.02, 133.32, 129.88, 126.05, 123.04, 119.14, 115.14, 112.96, 49.67, 20.53 ppm.

2-{2-[(4-(Trifluoromethyl)phenyl)amino]acetamide}benzoic acid (7c): A solution of **6a** (3.0 g, 11.6 mmol) and 4-trifluoromethylaniline (2.34 g, 1.82 mL, 14.5 mmol, 1.25 equiv) in CH_3CN (50 mL) was held at reflux for 18 h. After this period the solution was cooled in an ice bath to precipitate. The solid was collected by filtration, washed with ice-CH_3CN and dried to give 2.07 g (53%) of **7c** as a white solid; mp: 218–221 °C. ^{1}H NMR (400 MHz, DMSO): δ = 11.94 (s, 1H), 8.70 (d, J = 8.4 Hz, 1H), 7.94 (dd, J = 7.9, 1.5 Hz, 1H), 7.61 (dd, J = 7.9, 7.7 Hz, 1H), 7.43 (d, J = 8.6 Hz, 2H), 7.42 (s, 1H) 7.15 (dd, J = 7.7, 7.4 Hz, 1H), 6.73 (d, J = 8.6 Hz, 2H), 3.95 ppm (s, 2H); ^{13}C NMR (100 MHz, DMSO): δ = 170.39, 169.68, 151.61, 140.92, 134.70, 131.61, 126.81, 123.29, 119.86, 116.38, 112.41, 48.53 ppm; ^{19}F NMR (376 MHz, DMSO): δ = −59.09 ppm (s).

2-{2-[(4-(Nitro)phenyl)amino]acetamide}benzoic acid (7d): A solution of **6a** (3.0 g, 11.6 mmol) and 4-nitroaniline (3.21 g, 23.2 mmol, 2 equiv) in DMF (30 mL) was held at reflux for 66 h according to general procedure B to give 2.22 g (60%) of **7d** as a yellow solid; mp: 231–235 °C. ^{1}H NMR (400 MHz, DMSO): δ = 11.81 (s, 1H), 8.66 (d, J = 8.1 Hz, 1H), 8.04 (d, J = 9.3 Hz, 2H), 7.95 (dd, J = 8.0, 1.5 Hz, 1H), 7.61 (dd, J = 9.3, 7.7 Hz, 1H), 7.16 (dd, J = 8.1, 7.7 Hz, 1H), 6.74 (d, J = 9.3 Hz, 2H), 4.10 ppm (s, 2H); ^{13}C NMR (100 MHz, DMSO): δ = 169.79, 169.37, 154.54, 140.85, 137.47, 134.73, 131.63, 126.55, 123.42, 119.98, 116.52, 112.07, 48.06 ppm.

2-{2-[(4-(Ethoxycarbonyl)phenyl)amino]acetamide}benzoic acid (7e): A solution of **6a** (5.0 g, 19.4 mmol) and ethyl 4-aminobenzoate (9.6 g, 58.1 mmol, 3.5 equiv) in DMF (30 mL) was held at reflux for 96 h according to general procedure B to give 2.70 g (40%) of **7e** as a light-yellow solid; mp: >330 °C. ^{1}H NMR (400 MHz, MeOD): δ = 8.69 (d, J = 8.4, 1H), 8.03 (dd, J = 7.9, 1.5, 1H), 7.82 (d, J = 8.8, 2H), 7.56 (t, J = 7.1, 1H), 7.14 (t, J = 7.2, 1H), 6.68 (d, J = 8.8, 2H), 4.28 (q, J = 7.1, 2H), 4.02 (s, 2H), 1.35 ppm (t, J = 7.1, 3H); ^{13}C NMR (100 MHz, MeOD): δ = 170.93, 169.12, 167.27, 152.16, 140.22, 133.66, 131.10, 130.93, 122.84, 119.83, 118.64, 116.41, 111.50, 60.04, 48.45, 13.30 ppm.

General procedure C: 5*H*-indolo[3,2-*b*]quinolin-11(10*H*)-one (8a): A mixture **7a** (6.0 g, 21.5 mmol) and polyphosphoric acid (PPA, 160 g) was heated with mechanical stirring at 130 °C for 2 h. The reaction mixture was added to ice-water (500 mL), neutralised with saturated KOH solution, and then extracted with EtOAc (3× 500 mL). The extract was washed with H_2O, dried with brine and anhydrous Na_2SO_4, and then the solvent was removed at reduced pressure. The product was recrystallised from EtOAc with Et_2O/hexane (9:1) to give 3.47 g (67%) of **8a** as a light-green solid; mp: >300 °C. ^{1}H NMR (400 MHz, DMSO): δ = 12.81 (s, 1H), 11.69 (s, 1H), 8.35 (d, J = 8.0 Hz, 1H), 8.28 (d, J = 8.0 Hz, 1H), 7.81 (d, J = 8.4 Hz, 1H), 7.68 (dd, J = 8.4, 7.5 Hz, 1H), 7.50 (d, J = 8.2, 1H), 7.49 (dd, J = 8.2, 7.4 Hz, 1H), 7.28 (dd, J = 8.0, 7.5 Hz, 1H), 7.20 ppm (dd, J = 8.0, 7.4 Hz, 1H); ^{13}C NMR (100 MHz, DMSO): δ = 167.77, 139.54, 139.05, 130.99, 129.44, 127.84, 125.57, 123.48, 123.24, 121.63, 120.87, 119.25, 118.28, 116.38, 112.98 ppm.

3-Chloro-7-methyl-5*H*-indolo[3,2-*b*]quinolin-11(10*H*)-one (8b): Reaction of **7b** (1.5 g, 4.7 mmol) with PPA (45 g) according to general procedure C gave 0.697 g (52%) of **8b**, as a light-green solid; mp: >300 °C. ^{1}H NMR (400 MHz, DMSO): δ = 12.53 (s, NH), 11.67 (s, NH), 8.33 (d, J = 8.7 Hz, 1H), 7.92 (s, 1H), 7.72 (d, J = 1.7 Hz, 1H), 7.42 (d, J = 8.5 Hz, 1H), 7.32 (d, J = 8.5 Hz, 1H), 7.28 (dd, J = 8.7, 1.7 Hz, 1H), 2.47 ppm (s, 3H); ^{13}C NMR (100 MHz, DMSO): δ = 167.23, 139.98, 137.57, 135.55, 129.89, 129.05, 128.31, 127.92, 123.86, 121.88, 121.19, 120.33, 117.07, 116.24, 112.95, 21.61 ppm.

11-Oxo-10,11-dihydro-5*H*-indolo[3,2-*b*]quinoline-7-carboxylic acid (8c): Reaction of **7c** (2.0 g, 6.1 mmol) with PPA (60 g) according to general procedure C gave 0.312 g (19%) of **8c** as a light-brown solid. Reaction of **7e** (2.0 g, 5.8 mmol) with PPA (60 g) according to general procedure C gave 1.01 g (62%) of **8c** as a light-brown solid; mp: >300 °C. ^{1}H NMR (400 MHz, DMSO): δ = 12.64 (s, 1H), 12.10 (s, 1H), 8.99 (s, 1H), 8.36 (d, J = 7.9 Hz, 1H), 8.04 (dd, J = 8.7, 1.6 Hz, 1H), 7.72 (m, 2H), 7.56 (d, J = 8.7 Hz, 1H), 7.32 ppm (dd, J = 7.9, 7.1 Hz, 2H); ^{13}C NMR (100 MHz, DMSO): δ = 168.18, 167.92, 141.01, 139.60, 131.44, 130.07, 128.55, 125.64, 124.60, 124.20, 123.54, 121.80, 121.29, 118.37, 116.18, 112.77 ppm; MS ESI$^+$ (m/z) calcd for $C_{16}H_{10}N_2O_3$: 278.06, found: 278.96.

2-Hydroxy-3-((4-nitrophenyl)amino)quinolin-4(1*H*)-one (7id): Compound **7d** (2.0 g, 6.34 mmol) was reacted in PPA (60 g) for 2 h at 130 °C according with general procedure C to give a yellow solid (0.701 g), to yield **7id** at 37%; mp: 225–229 °C. ^{1}H NMR (400 MHz, DMSO): δ = 12.86 (s, 1H), 10.54 (s, 1H), 8.70 (d, J = 8.4 Hz, 1H), 8.07 (dd, J = 7.9, 1.5 Hz, 1H), 7.68 (dd, J = 7.9, 7.7 Hz, 1H), 7.52 (d, J = 8.8 Hz, 2H), 7.25 (dd, J = 8.4, 7.7 Hz, 1H), 6.56 ppm (d, J = 8.8 Hz, 2H); ^{13}C NMR (100 MHz, DMSO): δ = 169.40, 159.29, 157.46, 146.41, 139.76, 134.46, 131.93, 126.93, 124.23, 122.35, 119.90, 118.25, 114.06 ppm; MS ESI$^+$ (m/z) calcd for $C_{15}H_{11}N_3O_4$: 297.07, found: 298.10.

General procedure D. 5,10-Bis(2-(pyrrolidin-1-yl)ethyl)-5*H*-indolo[3,2-*b*]quinolin-11(10*H*)-one (3a) and 11-(2-(pyrrolidin-1-yl)ethoxy)-10-(2-(pyrrolidin-1-yl)ethyl)-10*H*-indolo[3,2-*b*]quinolone (4a): A solution of **8a** (70 mg, 0.29 mmol), K_2CO_3 (619.8 mg, 4.35 mmol, 15 equiv), in dried acetone (20 mL) and 1-(2-chloroethyl)pyrrolidine hydrochloride (203.4 mg, 1.20 mmol, 4 equiv) was held at reflux overnight. After this period, the solvent was removed at reduced pressure, and the remaining solid suspended in H_2O

(30 mL). The aqueous solution was extracted with CH_2Cl_2 (3× 30 mL), and the combined organic extracts were washed with H_2O, dried with brine and anhydrous Na_2SO_4, and decreased to small volume. The crude mixture was purified by preparative TLC using CH_2Cl_2/MeOH (9:1) as eluent to afford compounds **3a** (27.3 mg, 21%) and **4a** (45.5 mg, 35%). The compounds were recrystallised as hydrochloride salts with HCl in Et_2O after NMR characterisation and obtained as light-yellow solids. **3a**: mp: 227–230 °C; ^{1}H NMR (400 MHz, $CDCl_3$): δ = 8.68 (d, J = 7.8 Hz, 1H), 8.24 (d, J = 8.4 Hz, 1H), 7.72 (m, 2H), 7.69 (d, J = 8.5 Hz, 1H), 7.57 (dd, J = 8.5, 7.2 Hz, 1H), 7.37 (ddd, J = 7.8 Hz, 1H), 7.28 (dd, J = 8.4, 7.2 Hz, 1H), 5.13 (t, J = 7.7 Hz, 2H), 4.89 (t, J = 7.8 Hz, 2H), 3.11 (m, 4H), 2.85 (m, 4H), 2.78 (m, 4H), 1.92 (m, 4H), 1.89 ppm (m, 4H); ^{13}C NMR (100 MHz, $CDCl_3$): δ = 169.05, 139.61, 139.51, 131.62, 130.81, 127.70, 126.78, 124.88, 122.50, 122.46, 121.18, 119.95, 115.10, 114.11, 110.65, 55.82, 54.75, 54.24, 53.44, 47.20, 43.21, 23.62, 23.58 ppm; Anal. calcd for $C_{27}H_{32}N_4O{\cdot}2HCl{\cdot}2H_2O$: C 60.33, H 7.13, N 10.42, found: C 60.76, H 7.53, N 10.32. **4a**: mp: 212–216 °C; ^{1}H NMR (400 MHz, $CDCl_3$): δ = 8.44 (d, J = 7.6 Hz, 1H), 8.22 (d, J = 8.0 Hz, 1H), 8.20 (d, J = 8.0 Hz, 1H), 7.62–7.54 (m, 2H), 7.49 (d, J = 8.0 Hz, 1H), 7.48 (dd, J = 8.0, 8.0 Hz, 1H) 7.25 (ddd, 1H), 4.79 (t, J = 7.5 Hz, 2H), 4.30 (t, J = 5.8 Hz, 2H), 3.03 (t, J = 5.8 Hz, 2H), 2.86 (t, J = 7.5 Hz, 2H), 2.63 (m, 8H), 1.79 (m, 4H), 1.75 ppm (m, 4H); ^{13}C NMR (100 MHz, $CDCl_3$): δ = 148.59, 145.92, 144.58, 144.43, 129.95, 129.37, 126.78, 124.88, 124.62, 122.41, 122.14, 122.09, 121.10, 120.13, 109.24, 74.64, 55.81, 54.76, 54.41, 43.43, 23.60, 23.56 ppm; Anal. calcd for $C_{27}H_{32}N_4O{\cdot}2HCl{\cdot}3H_2O$: C 58.37, H 7.26, N 10.09, found: C 58.79, H 7.74, N 9.72.

5,10-Bis(3-(piperidin-1-yl)propyl)-5*H*-indolo[3,2-*b*]quinolin-11(10*H*)-one (**3b**) **and 11-(3-(piperidin-1-yl)propoxy)-10-(3-(piperidin-1-yl)propyl)-10*H*-indolo[3,2-*b*]quinoline** (**4b**): A solution of **8a** (70 mg, 0.29 mmol), K_2CO_3 (619.8 mg, 4.35 mmol, 15 equiv), in dried acetone (20 mL) and 1-(3-chloropropyl)piperidine hydrochloride (237.0 mg, 1.20 mmol, 4 equiv) was reacted and purified according to general procedure D to give **3b** (45.2 mg, 31%) and **4b** (56.3 mg, 38%) as light-yellow solids. **3b**: mp: 258–261 °C; ^{1}H NMR (400 MHz, $CDCl_3$): δ = 8.68 (d, J = 8.1 Hz, 1H), 8.24 (d, J = 8.3 Hz, 1H), 7.80 (d, J = 8.6 Hz, 1H), 7.68 (dd, J = 8.6, 7.3 Hz, 1H), 7.65 (d, J = 8.4 Hz, 1H), 7.52 (dd, J = 8.4, 7.4 Hz, 1H), 7.34 (dd, J = 8.1, 7.3 Hz, 1H), 7.22 (dd, J = 8.3, 7.4 Hz, 1H), 4.96 (t, J = 7.1 Hz, 2H), 4.81 (t, J = 7.2 Hz, 2H), 2.53 (t, J = 6.3 Hz, 2H), 2.47 (m, 4H), 2.35 (m, 6H), 2.18 (m, 2H), 2.12 (quint, J = 7.1 Hz, 2H), 1.69 (quint, J = 5.5 Hz, 4H), 1.58 (quint, J = 5.6 Hz, 4H), 1.51 (m, 2H), 1.42 ppm (m, 2H); ^{13}C NMR (100 MHz, $CDCl_3$): δ = 169.03, 139.79, 139.53, 131.21, 130.66, 127.05, 126.73, 124.91, 122.73, 122.70, 120.84, 119.33, 115.08, 114.37, 110.91, 55.97, 55.91, 55.07, 54.54, 54.46, 53.83, 46.25, 42.78, 28.19, 26.20, 25.98, 24.48 ppm; Anal. calcd for $C_{31}H_{40}N_4O{\cdot}2HCl{\cdot}5H_2O$: C 57.49, H 8.09, N 8.65, found: C 57.45, H 8.04, N 8.43. **4b**: mp: 241–245 °C; ^{1}H NMR (400 MHz, $CDCl_3$): δ = 8.53 (d, J = 7.7 Hz, 1H), 8.32 (d, J = 7.9 Hz, 1H), 8.31 (d, J = 7.8 Hz, 1H), 7.66–7.58 (m, 2H), 7.53 (dd, J = 8.4, 7.8 Hz, 1H), 7.51 (d, J = 7.8 Hz, 1H), 7.30 (dd, J = 7.7, 7.2 Hz, 1H), 4.57 (t, J = 6.9 Hz, 2H), 4.22 (t, J = 6.2 Hz, 2H), 2.65 (t, J = 7.2 Hz, 2H), 2.47 (m, 4H), 2.26 (m, 6H), 2.20 (quint, J =, 6.2 Hz, 2H), 2.02 (quint, J = 6.9 Hz, 2H), 1.64 (quint, J = 5.6 Hz, 4H), 1.54 (quint, J = 5.6 Hz, 4H), 1.49 (m, 2H), 1.40 ppm (m, 2H); ^{13}C NMR (100 MHz, $CDCl_3$): δ = 148.58, 145.76, 144.82, 144.53, 129.54, 129.29, 126.55, 124.74, 124.59, 122.34, 122.18, 121.92, 121.25, 119.68, 109.36, 74.13, 56.12, 55.35, 54.68, 54.53, 42.75, 27.58, 26.91, 26.09, 25.97, 24.52, 24.45 ppm; Anal. calcd for $C_{31}H_{40}N_4O{\cdot}3HCl{\cdot}3.5H_2O$: C 56.36, H 8.01, N 8.55, found: C 56.66, H 7.67, N 8.53.

3-Chloro-5,10-bis(2-(diethylamino)ethyl)-7-methyl-5*H*-indolo[3,2-*b*]quinolin-11(10*H*)-one (**3c**) **and 2-((3-chloro-10-(2-(diethylamino)ethyl)-7-methyl-10*H*-indolo[3,2-*b*]quinolin-11-yl)oxy)-*N*,*N*-diethylethanamine** (**4c**): A solution of **8b** (80 mg, 0.28 mmol), K_2CO_3 (580 mg, 4.20 mmol, 15 equiv), in dried acetone (20 mL) and 2-chloro-N^1,N^1-diethylethanaminium chloride (192.7 mg, 1.12 mmol, 4 equiv) was reacted and purified according to general procedure D to give **3c** (26.3 mg, 19%) and **4c** (47.2 mg, 35%) as light-yellow solids. **3c**: mp: 220–222 °C; ^{1}H NMR (400 MHz, $CDCl_3$): δ = 8.36 (d, J = 8.7 Hz, 1H), 7.77 (s, 1H), 7.48 (d, J = 1.6 Hz, 1H), 7.28 (d, J = 8.6 Hz, 1H), 7.17 (d, J = 8.6 Hz, 1H), 7.05 (dd, J = 8.7, 1.67 Hz, 1H), 4.74 (t, J = 7.2 Hz, 2H), 4.54 (t, J = 7.2 Hz, 2H), 2.81 (t, J = 7.2 Hz, 2H), 2.68 (t, J = 7.2 Hz, 2H), 2.51 (q, J = 7.1 Hz, 4H), 2.48 (q, J = 7.1 Hz, 4H), 2.32 (s, 3H), 0.90 (t, J = 7.1 Hz, 6H), 0.85 ppm (t, J = 7.1 Hz, 6H); ^{13}C NMR (100 MHz, $CDCl_3$): δ = 168.55, 140.29, 138.29, 137.60, 130.23, 129.42, 129.11, 128.44, 123.17, 122.96, 121.77, 121.51, 115.10, 114.16, 110.45, 53.13, 50.86, 47.77, 47.57, 43.06, 21.62, 12.05, 11.97 ppm; Anal. calcd for $C_{28}H_{37}N_4O{\cdot}2HCl{\cdot}3.5H_2O$: C 54.50, H 7.51, N 9.08, found: C 54.60, H 7.57, N 9.31. **4c**: mp: 254–256 °C; ^{1}H NMR (400 MHz, $CDCl_3$): δ = 8.27 (d, J = 9.0 Hz, 1H), 8.20 (s, 1H), 8.19 (d, J = 2.1 Hz, 1H), 7.40–7.36 (m, 2H)„ 7.29 (d, J = 8.4 Hz, 1H), 4.54 (t, J = 7.6 Hz, 2H), 4.16 (t, J = 6.1 Hz, 2H), 2.94 (t, J = 6.1 Hz, 2H), 2.66 (t, J = 7.6 Hz, 2H), 2.58 (q, J = 7.1 Hz, 4H), 2.50 (q, J = 7.1 Hz, 4H), 2.47 (s, 3H), 1.01 (t, J = 7.1 Hz, 6H), 0.88 ppm (t, J = 7.1 Hz, 6H); ^{13}C NMR (100 MHz, $CDCl_3$): δ = 149.39, 145.91, 144.55, 143.27, 132.18, 131.37, 129.57, 127.97, 125.41, 125.21, 122.84, 122.32, 121.98, 120.65, 109.02, 74.82, 53.04, 51.71, 47.71, 47.63, 43.60, 21.16, 12.11, 11.91 ppm; Anal. calcd for $C_{28}H_{37}N_4O{\cdot}2HCl$: C 60.70, H 7.10, N 10.11, found: C 60.48, H 6.97, N 9.87.

2-(Diethylamino)ethyl 5,10-bis(2-(diethylamino)ethyl)-11-oxo-10,11-dihydro-5*H*-indolo[3,2-*b*]quinoline-7-carboxylate (**3d**) **and 2-(diethylamino)ethyl 11-(2-(diethylamino)ethoxy)-10-(2-(diethylamino)ethyl)-10*H*-indolo[3,2-*b*]quinoline-7-carboxylate** (**4d**): A solution of **8c** (70 mg, 0.23 mmol), K_2CO_3 (476 mg, 3.45 mmol, 15 equiv), in dried acetone (20 mL) and 2-chloro-N^1,N^1-diethylethanaminium chloride (159.3 mg, 0.92 mmol, 4 equiv) was reacted and purified according to general procedure D to give **3d** (36.2 mg, 31%) and **4d** (39.6 mg, 34%) as light-yellow solids. **3d**: mp: 175–178 °C; ^{1}H NMR (400 MHz, $CDCl_3$): δ = 9.00 (s, 1H), 8.65 (d, J = 8.0 Hz, 1H), 8.19 (d, J = 8.9 Hz, 1H), 7.72 (m, 2H), 7.60 (d, J = 8.9 Hz, 1H), 7.35 (m, 1H), 5.00 (t, J = 6.9 Hz, 2H), 4.87 (t, J = 6.7 Hz, 2H), 4.46 (t, J = 6.5 Hz, 2H), 3.03 (t, J = 6.7 Hz, 2H), 2.94 (t, J = 6.9 Hz, 2H), 2.91 (t, J = 6.5 Hz, 2H), 2.74 (q, J = 7.1 Hz, 4H), 2.68 (m, 8H), 1.10 (m, 12H), 1.04 ppm (t, J = 7.2 Hz, 6H); ^{13}C NMR (100 MHz, $CDCl_3$): δ = 169.05, 166.79, 141.65, 139.69, 131.74, 131.34, 128.08, 126.75, 125.84, 125.09, 123.16, 121.55, 121.43, 114.88, 114.43, 110.37, 63.18, 53.12, 51.16, 50.81, 47.79, 47.60, 47.49, 47.30, 43.36, 12.01, 11.89, 11.78 ppm; Anal. calcd for $C_{34}H_{49}N_5O_3{\cdot}3HCl{\cdot}3.5H_2O$: C 54.58, H 7.95, N 9.36, found: C 54.67, H 8.01, N 9.27. **4d**: mp: 168–172 °C; ^{1}H NMR (400 MHz, $CDCl_3$): δ = 9.24 (d, J = 1.5 Hz, 1H), 8.39 (dd, J = 8.4, 0.9 Hz, 1H), 8.35 (dd, J = 8.6, 1.7 Hz, 1H), 8.33 (d, J = 7.5 Hz, 1H), 7.71 (ddd, J = 8.4, 6.7, 1.4 Hz, 1H), 7.59 (ddd, J = 8.4, 6.8, 1.4 Hz, 1H), 7.52 (d, J = 8.7 Hz, 1H), 4.73 (t, J = 6.8 Hz, 2H), 4.49 (t, J = 6.6 Hz, 2H), 4.31 (t, J = 6.2 Hz, 2H), 3.08 (t, J = 6.2 Hz, 2H), 2.96 (t, J = 6.6 Hz, 2H), 2.83 t, J = 6.8 Hz, 2H), 2.70 (q, J = 7.2 Hz, 8H), 2.57 (q, J = 7.1 Hz, 4H), 1.13 (t, J = 7.2 Hz, 6H), 1.11 (t, J = 7.2 Hz, 6H), 0.93 ppm (t, J = 7.1 Hz, 6H); ^{13}C NMR (100 MHz, $CDCl_3$): δ = 166.84, 148.13, 147.36, 146.30, 145.15, 131.15, 129.46, 127.18, 125.30, 125.08, 124.39, 122.36, 122.16, 121.84, 121.40, 108.95, 74.79, 62.86, 52.97, 51.96, 51.12, 47.77, 47.65, 47.56, 43.88, 12.02, 11.90, 11.83 ppm; Anal. calcd for $C_{34}H_{49}N_5O_3{\cdot}3HCl{\cdot}2H_2O$: C 56.62, H 7.83, N 9.71, found: C 56.44, H 7.99, N 9.73.

FRET melting assays

The ability of indolo[3,2-*b*]quinolines to stabilise G-quadruplex DNA sequences was investigated by using a fluorescence resonance energy transfer (FRET) assay. The labelled oligonucleotides (Eurogentec Ltd., UK) contained the donor fluorophore 6-carboxyfluorescein (FAM) and the acceptor fluorophore 6-carboxytetramethylrhodamine (TAMRA). Sequences were as follows: F21T (5′-[FAM]-GGG TTA GGG TAG GGT TAG GG-[TAMRA]-3′), *KRas21R* (5′-[FAM]-AGG GCG GTG TGG GAA GAG GGA-[TAMRA]-3′), *Hsp90A* (5′-[FAM]-GGG CCA AAG GGA AGG GGT GGG-[TAMRA]-3′), *Hsp90C* (5′-[FAM]-AGG GCG GGC CAA AGG GAA GGG GTG GGC-[TAMRA]-3′), *c-Kit1* (5′-[FAM]-AGA GGG AGG GCG CTG GGA GGA GGG GCT-[TAMRA]-3′), *c-Kit2* (5′-[FAM]-CCC GGG CGG GCG CGA GGG AGG GGA GG-[TAMRA]-3′), *HIF-1α* (5′-[FAM]-GCG CGG GAG GGG AGA GGG GGC GGG AGC GCG-[TAMRA]-3′), T-loop (5′-[FAM]-TAT AGC TAT ATT TTT TTA TAG CTA TA-[TAMRA]-3′). Each oligonucleotide was initially diluted to 100 μM in nuclease-free water (not DEPC-treated), purchased from Ambion Applied Biosystems (UK). Stock solutions of 20 μM and subsequent dilutions were obtained in FRET buffer (60 mM KCl, potassium cacodylate, pH 7.4). The FRET probe sequences were diluted from stock to the correct concentration (0.4 μM) and then annealed by heating at 85 °C for 10 min, followed by slow cooling to room temperature in the heating block. Test compounds were prepared as 10 mM DMSO stock solutions and diluted to 1 mM using 1 mM HCl in HPLC-grade water. The rest of the dilutions were performed using FRET buffer. Annealed DNA (50 μL) and test compound solution (50 μL) were distributed across 96-well RT-PCR plates (BioRad; MJ Research, Waltham, MA, USA). Relevant controls were also performed to check for interference with the assay. Fluorescence readings were made with excitation at λ 450–495 nm and detection at λ 515–545 nm, taken at intervals of 0.5 °C in the range 30–100 °C, with a constant temperature being maintained for 30 s prior to each reading to ensure a stable value. The melting of the F21T G-quadruplex (0.2 μM) was also monitored in a competition assay in the presence of 0.4, 2.0, 10, and 25 μM non-fluorescent double-stranded competitor 26ds DNA (5′-CAA TCG GAT CGA ATT CGA TCC GAT TG-3′) at a ligand concentration of 1 μM. Experiments were performed in triplicate. Final analysis of the data was carried out with GraphPad Prism v.5.0 (GraphPad Software Inc., La Jolla, CA, USA). The advanced curve-fitting function in GraphPad Prism was used for calculation of ΔT_m values and associated standard deviations.

Molecular modelling studies

Molecular dynamics: G4 structures obtained from the RSCB Protein Data Bank (PDB IDs 1KF1, 143D, 2JPZ) were prepared in the MOE v.2012.10 software package (Chemical Computing Group)[35] by removing water molecules, adding the missing hydrogen atoms, and assigning protonation states with the Protonate 3D application tool by using the GB/VI formalism at 300 K, pH 7, and salt concentration of 0.1 M. Addition of the two K^+ ions to the G4 structures resolved by NMR were made by using the solvate application tool present in MOE v.2012.10 which, when necessary, were placed manually in the central cavity of the G4 structure. The systems were then subjected to MD simulations using the GROMACS simulation package 4.5.5[37] and applying the AMBER03[38] force field. The G4 structures prepared in MOE were inserted in a cubic box, with no less than 1 nm between the G4 and the simulation box edge. The system was solvated and neutralised by adding the required K^+ ions. After energy minimisation of the MD box with the steepest descent method, a 100 ps *NVT* equilibration run followed at 298 K (spatially restraining the oligonucleotide's heavy atoms). Finally, the dynamics of the system was studied by sampling the *NpT* ensemble ($T = 298$ K, $p = 1$ bar) for 10 ns. In all MD runs, the particle mesh Ewald (PME) formalism was applied in the long-range electrostatic interactions. The short-range electrostatic cutoff was 1.2 nm, and the same was applied for the van der Waals (vdW) interactions. All bonds were constrained with the Lincs algorithm. Nosé–Hoover and Parrinello–Rahman were applied to control the temperature and isotropic pressure ($\tau_T = 0.2$, $\tau_p = 5.0$ ps, and $\beta = 4.5 \times 10^{-5}$ bar^{-1}). Energy and pressure corrections for the vdW cutoff were also applied. The structures obtained at the end of these production runs were used in the docking studies and were visually compared with the starting PDB structures by using the alignment application tool present in MOE.

Docking: The crystal structure of the parallel-stranded F21T quadruplex (PDB ID 3CE5)[12b] was prepared with the MOE v.2012.10 software package by removing water and adding the missing hydrogen atoms and protonation states with Protonate 3D application tool, at 300 K, pH 7, salt concentration of 0.1 M at the GB/VI electrostatic formalism. The co-crystallised ligand found in PDB 3CE5 was re-docked with the G4 structure using rigid docking protocol, the triangle matcher placement, the alpha HB free-energy scoring function, and retaining 100 poses. Final poses were subjected to a final refinement in the receptor pocket with the AMBER99 force field, at an RMS gradient threshold of 0.01 and a second rescoring with alpha HB free-energy scoring function. The best-scoring values were selected as final poses. Indolo[3,2-*b*]quinoline ligand structures were also constructed in MOE and energy minimised with the MMFF94x force field at an RMS gradient threshold of 0.05. The refined parallel, antiparallel basket, and hybrid G4 structures (1KF1, 143D, and 2JPZ, respectively) obtained from the MD simulations were used in docking with the indolo[3,2-*b*]quinolone ligands as described above. The G4–ligand interactions were visualised with the MOE v.2012.10 ligand interactions application tool.

Viability assays

HCT116 human colon carcinoma cells were grown in McCoy's 5A medium supplemented with 10% fetal bovine serum (FBS) and 1% antibiotic/antimycotic (Invitrogen, Grand Island, NY, USA) and maintained at 37 °C in a humidified atmosphere of 5% CO_2. Cells were seeded in 96-well plates at 5000 cells per well. Primary rat hepatocytes were isolated from male Sprague–Dawley rats (100–150 g) by collagenase perfusion as described previously.[39] Cell viability was determined by trypan blue exclusion and was typically 80–85%. After isolation, hepatocytes were resuspended in William's E medium and plated on Primaria 96-well culture plates (BD Biosciences, San Jose, CA, USA) at 5000 cells per well. The cells were maintained at 37 °C in a humidified atmosphere of 5% CO_2 for 4 h to allow attachment. Plates were then washed with medium to remove dead cells and incubated in William's E medium containing 10% heat-inactivated FBS. Test compounds **3d** and **4d**, and the positive control 5-fluorouracil (5-FU, Sigma), a common cytotoxic agent used in colon cancer treatment,[40] were dissolved in DMSO; 24 h after cell plating, media was removed and replaced with fresh media containing 1–100 μM test compounds and 5-FU, or vehicle (DMSO) control. After compound exposure for 96 h, cell viability was evaluated using CellTiter 96 AQueous Non-Radioactive Cell Proliferation Assay (Promega, Madison, WI, USA), using 3-(4,5-dimethylthiazol-2-yl)-5-(3-carboxymethoxyphenyl)-2-(4-sulfophenyl)-2*H*-tetrazolium, inner salt (MTS) as previously described.[41] Cell viability data were expressed as mean ± SEM or mean ± SD from at least three independent experiments. IC_{50} and IC_{90} values were determined using GaphPad Prism v.5.00 (GraphPad Software).

Total protein extraction and immunoblotting

HCT116 cells were seeded in 35 mm plates at 150000 cells per well. Test compounds **3d** and **4d** were dissolved in DMSO and added to the cells 24 h after plating, at IC_{50}, 10, and 20 μM. Vehicle (DMSO) control was also included. After compound exposure for 72 h, cells were collected and processed for total protein extraction. Briefly, samples were homogenised in ice-cold 1:1 solution of buffer A [10 mM Tris·HCl pH 7.6, 5 mM $MgCl_2$, 1.5 mM KOAc, 2 mM dithiothreitol (DTT), and Halt Protease and Phosphatase inhibitor cocktail, EDTA-free (#78445, Thermo Scientific)] and buffer 2× (10 mM Tris·HCl pH 7.6, 1% Nonidet-P40, and Halt Protease and Phosphatase inhibitor cocktail), by vigorous vortexing and incubated on ice for 30 min. Samples were then sonicated (two cycles of 15 s sonication and 30 s ice incubation, using a compact ultrasonic device with amplitude adjusted to 80% and pulse to 90%; model UP100H, Hielscher Ultrasonics GmbH, Teltow (Germany); 100 W, ultrasonic frequency: 30 kHz) and centrifuged at 10000 *g* for 10 min at 4 °C. The clear supernatants containing the total protein extracts were transferred to a fresh tube and stored at −80 °C. Protein concentrations were determined using the BioRad protein assay kit according to the manufacturer's instructions.[40b,42] Steady-state levels of Hsp90 and KRas proteins were determined by immunoblot analysis. Briefly, 25 μg of total protein extracts were separated by 10% SDS-PAGE. After electrophoretic transfer onto nitrocellulose membranes, immunoblots were incubated with 15% H_2O_2 for 15 min at room temperature. After blocking with 5% milk solution, the blots were incubated overnight at 4 °C with primary mouse monoclonal antibody reactive to Hsp90 or to KRas (#13119 and #sc-30, respectively; Santa Cruz Biotechnology Inc., Santa Cruz, CA, USA). Finally, membranes were incubated with secondary anti-mouse sera conjugated with horseradish peroxidase (BioRad) for 3 h at room temperature. The membranes were processed for protein detection using Super Signal substrate (Pierce, Rockford, IL, USA). β-Actin (#A-5441, Sigma–Aldrich) was used as a loading control. Protein levels were expressed as mean ±SEM from at least three independent experiments.

Acknowledgements

The authors thank the Fundação para a Ciencia e Tecnologia (FCT), Portugal, for financial support through project grants PEst-OE/SAU/UI4013/2011, EXPL/QEQ-MED/0502/2012, and PTDC/SAU-ORG/119842/2010. J.L. also acknowledges the FCT for a postdoctoral grant: SFRH/BPD/72903/2010. Work in London was supported by Cancer Research UK.

Keywords: alkaloids · cancer · cryptolepine · G-quadruplexes · indoloquinolines

[1] S. Neidle, *Curr. Opin. Struct. Biol.* **2009**, *19*, 239 – 250.
[2] A. K. Todd, M. Johnston, S. Neidle, *Nucleic Acids Res.* **2005**, *33*, 2901 – 2907.
[3] a) S. Balasubramanian, L. H. Hurley, S. Neidle, *Nat. Rev. Drug Discovery* **2011**, *10*, 261 – 275; b) S. Neidle, *FEBS J.* **2010**, *277*, 1118 – 1125.
[4] L. Neckers, P. Workman, *Clin. Cancer Res.* **2012**, *18*, 64 – 76.
[5] S. A. Ohnmacht, M. Micco, V. Petrucci, A. K. Todd, A. P. Reszka, M. Gunaratnam, M. A. Carvalho, M. Zloh, S. Neidle, *Bioorg. Med. Chem. Lett.* **2012**, *22*, 5930 – 5935.
[6] T. A. Brooks, L. H. Hurley, *Genes Cancer* **2010**, *1*, 641 – 649.
[7] a) M. Gunaratnam, S. Swank, S. M. Haider, K. Galesa, A. P. Reszka, M. Beltran, F. Cuenca, J. A. Fletcher, S. Neidle, *J. Med. Chem.* **2009**, *52*, 3774 – 3783; b) K. I. E. McLuckie, Z. A. E. Waller, D. A. Sanders, D. Alves, R. Rodriguez, J. Dash, G. J. McKenzie, A. R. Venkitaraman, S. Balasubramanian, *J. Am. Chem. Soc.* **2011**, *133*, 2658 – 2663.
[8] S. Cogoi, L. E. Xodo, *Nucleic Acids Res.* **2006**, *34*, 2536 – 2549.
[9] M. Gunaratnam, M. de La Fuente, S. M. Hampel, A. K. Todd, A. P. Reszka, A. Schatzlein, S. Neidle, *Bioorg. Med. Chem.* **2011**, *19*, 7151 – 7157.
[10] a) Y. Xu, *Chem. Soc. Rev.* **2011**, *40*, 2719 – 2740; b) J. H. Tan, L. Q. Gu, J. Y. Wu, *Mini-Rev. Med. Chem.* **2008**, *8*, 1163 – 1178.
[11] D. Z. Yang, K. Okamoto, *Future Med. Chem.* **2010**, *2*, 619 – 646.
[12] a) N. H. Campbell, M. Patel, A. B. Tofa, R. Ghosh, G. N. Parkinson, S. Neidle, *Biochemistry* **2009**, *48*, 1675 – 1680; b) N. H. Campbell, G. N. Parkinson, A. P. Reszka, S. Neidle, *J. Am. Chem. Soc.* **2008**, *130*, 6722 – 6724; c) J. Dai, M. Carver, L. H. Hurley, D. Yang, *J. Am. Chem. Soc.* **2011**, *133*, 17673 – 17680.
[13] a) J. Lavrado, R. Moreira, A. Paulo, *Curr. Med. Chem.* **2010**, *17*, 2348 – 2370; b) J. Lavrado, R. Moreira, A. Paulo, in *Heterocyclic Targets in Advanced Organic Synthesis* (Eds.: M. D. Carreiras, J. Marco-Contelles), Research Signpost, Kerala (India), 2011, pp. 109 – 124.; c) K. Görlitzer, J. Weber, *Arch. Pharm.* **1981**, *314*, 852 – 861; d) D. E. Bierer, L. G. Dubenko, P. Zhang, Q. Lu, P. A. Imbach, A. W. Garofalo, P. W. Phuan, D. M. Fort, J. Litvak, R. E. Gerber, B. Sloan, J. Luo, R. Cooper, G. M. Reaven, *J. Med. Chem.* **1998**, *41*, 2754 – 2764.
[14] a) T. M. Ou, Y. J. Lu, C. Zhang, Z. S. Huang, X. D. Wang, J. H. Tan, Y. Chen, D. L. Ma, K. Y. Wong, J. C. Tang, A. S. Chan, L. Q. Gu, *J. Med. Chem.* **2007**, *50*, 1465 – 1474; b) P. V. Boddupally, S. Hahn, C. Beman, B. De, T. A. Brooks, V. Gokhale, L. H. Hurley, *J. Med. Chem.* **2012**, *55*, 6076 – 6086; c) Y. J. Lu, T. M. Ou, J. H. Tan, J. Q. Hou, W. Y. Shao, D. Peng, N. Sun, X. D. Wang, W. B. Wu, X. Z. Bu, Z. S. Huang, D. L. Ma, K. Y. Wong, L. Q. Gu, *J. Med. Chem.* **2008**, *51*, 6381 – 6392; d) Z. S. Huang, T. M. Ou, J. Lin, Y. J. Lu, J. Q. Hou, J. H. Tan, S. H. Chen, Z. Li, Y. P. Li, D. Li, L. Q. Gu, *J. Med. Chem.* **2011**, *54*, 5671 – 5679.
[15] J. Lavrado, A. P. Reszka, R. Moreira, S. Neidle, A. Paulo, *Bioorg. Med. Chem. Lett.* **2010**, *20*, 7042 – 7045.
[16] B. Guyen, C. M. Schultes, P. Hazel, J. Mann, S. Neidle, *Org. Biomol. Chem.* **2004**, *2*, 981 – 988.
[17] Y. Kobayashi, I. Kumadaki, *Acc. Chem. Res.* **1978**, *11*, 197 – 204.
[18] J. Lavrado, G. G. Cabal, M. Prudencio, M. M. Mota, J. Gut, P. J. Rosenthal, C. Diaz, R. C. Guedes, D. J. Dos Santos, E. Bichenkova, K. T. Douglas, R. Moreira, A. Paulo, *J. Med. Chem.* **2011**, *54*, 734 – 750.
[19] J. Lavrado, K. Gani, P. A. Nobre, S. A. Santos, P. Figueiredo, D. Lopes, V. Rosario, J. Gut, P. J. Rosenthal, R. Moreira, A. Paulo, *Bioorg. Med. Chem. Lett.* **2010**, *20*, 5634 – 5637.
[20] C. M. Schultes, W. Guyen, J. Cuesta, S. Neidle, *Bioorg. Med. Chem. Lett.* **2004**, *14*, 4347 – 4351.
[21] J. Lavrado, A. Paulo, E. Bichenkova, K. T. Douglas, R. Moreira, *Magn. Reson. Chem.* **2012**, *50*, 216 – 220.
[22] a) M. J. Moore, C. M. Schultes, J. Cuesta, F. Cuenca, M. Gunaratnam, F. A. Tanious, W. D. Wilson, S. Neidle, *J. Med. Chem.* **2006**, *49*, 582 – 599; b) F. Cuenca, M. J. Moore, K. Johnson, B. Guyen, A. De Cian, S. Neidle, *Bioorg. Med. Chem. Lett.* **2009**, *19*, 5109 – 5113.
[23] G. W. Collie, R. Promontorio, S. M. Hampel, M. Micco, S. Neidle, G. N. Parkinson, *J. Am. Chem. Soc.* **2012**, *134*, 2723 – 2731.
[24] M. Paramasivam, S. Cogoi, L. E. Xodo, *Chem. Commun.* **2011**, *47*, 4965 – 4967.
[25] R. De Armond, S. Wood, D. Y. Sun, L. H. Hurley, S. W. Ebbinghaus, *Biochemistry* **2005**, *44*, 16341 – 16350.
[26] A. De Cian, L. Guittat, K. Shin-ya, J. F. Riou, J. L. Mergny, *Nucleic Acids Symp. Ser.* **2005**, *49*, 235 – 236.
[27] A. N. Lane, J. B. Chaires, R. D. Gray, J. O. Trent, *Nucleic Acids Res.* **2008**, *36*, 5482 – 5515.
[28] D. Renciuk, I. Kejnovska, P. Skolakova, K. Bednarova, J. Motlova, M. Vorlickova, *Nucleic Acids Res.* **2009**, *37*, 6625 – 6634.
[29] B. Heddi, A. T. Phan, *J. Am. Chem. Soc.* **2011**, *133*, 9824 – 9833.
[30] G. N. Parkinson, M. P. Lee, S. Neidle, *Nature* **2002**, *417*, 876 – 880.
[31] Y. Wang, D. J. Patel, *Structure* **1993**, *1*, 263 – 282.
[32] J. Dai, C. Punchihewa, A. Ambrus, D. Chen, R. A. Jones, D. Yang, *Nucleic Acids Res.* **2007**, *35*, 2440 – 2450.
[33] M. Cavallari, A. Calzolari, A. Garbesi, R. Di Felice, *J. Phys. Chem. B* **2006**, *110*, 26337 – 26348.
[34] B. Islam, M. Sgobba, C. Laughton, M. Orozco, J. Sponer, S. Neidle, S. Haider, *Nucleic Acids Res.* **2013**, *41*, 2723 – 2735.

[35] Molecular Operating Environment (MOE) v.2012.10, Chemical Computing Group Inc., 2012, Montreal, QC (Canada).
[36] S. Alcaro, A. Artese, J. N. Iley, S. Missailidis, F. Ortuso, L. Parrotta, R. Pasceri, F. Paduano, C. Sissi, F. Trapasso, M. G. Vigorita, *ChemMedChem* **2010**, *5*, 575 – 583.
[37] a) H. J. C. Berendsen, D. van der Spoel, R. van Drunen, *Comput. Phys. Commun.* **1995**, *91*, 43 – 56; b) E. Lindahl, B. Hess, D. van der Spoel, *J. Mol. Model.* **2001**, *7*, 306 – 317; c) D. van der Spoel, E. Lindahl, B. Hess, G. Groenhof, A. E. Mark, H. J. C. Berendsen, *J. Comput. Chem.* **2005**, *26*, 1701 – 1718.
[38] L. J. Yang, C. H. Tan, M. J. Hsieh, J. M. Wang, Y. Duan, P. Cieplak, J. Caldwell, P. A. Kollman, R. Luo, *J. Phys. Chem. B* **2006**, *110*, 13166 – 13176.
[39] R. E. Castro, S. Sola, X. Ma, R. M. Ramalho, B. T. Kren, C. J. Steer, C. M. Rodrigues, *J. Hepatol.* **2005**, *42*, 897 – 906.
[40] a) P. M. Borralho, I. B. Moreira da Silva, M. M. Aranha, C. Albuquerque, C. Nobre Leitao, C. J. Steer, C. M. Rodrigues, *Biochim. Biophys. Acta Mol. Basis Dis.* **2007**, *1772*, 40 – 47; b) P. M. Borralho, B. T. Kren, R. E. Castro, I. B. da Silva, C. J. Steer, C. M. Rodrigues, *FEBS J.* **2009**, *276*, 6689 – 6700.
[41] T. F. Silva, L. M. Martins, M. F. Guedes da Silva, A. R. Fernandes, A. Silva, P. M. Borralho, S. Santos, C. M. Rodrigues, A. J. Pombeiro, *Dalton Trans.* **2012**, *41*, 12888 – 12897.
[42] a) P. M. Borralho, A. E. Simoes, S. E. Gomes, R. T. Lima, T. Carvalho, D. M. Ferreira, M. H. Vasconcelos, R. E. Castro, C. M. Rodrigues, *PLoS One* **2011**, *6*, e23787; b) A. E. Simões, D. M. Pereira, J. D. Amaral, A. F. Nunes, S. E. Gomes, P. M. Rodrigues, A. C. Lo, R. D'Hooge, C. J. Steer, S. N. Thibodeau, P. M. Borralho, C. M. Rodrigues, *BMC Genomics* **2013**, *14*, 181.

Received: June 28, 2013
Published online on August 19, 2013